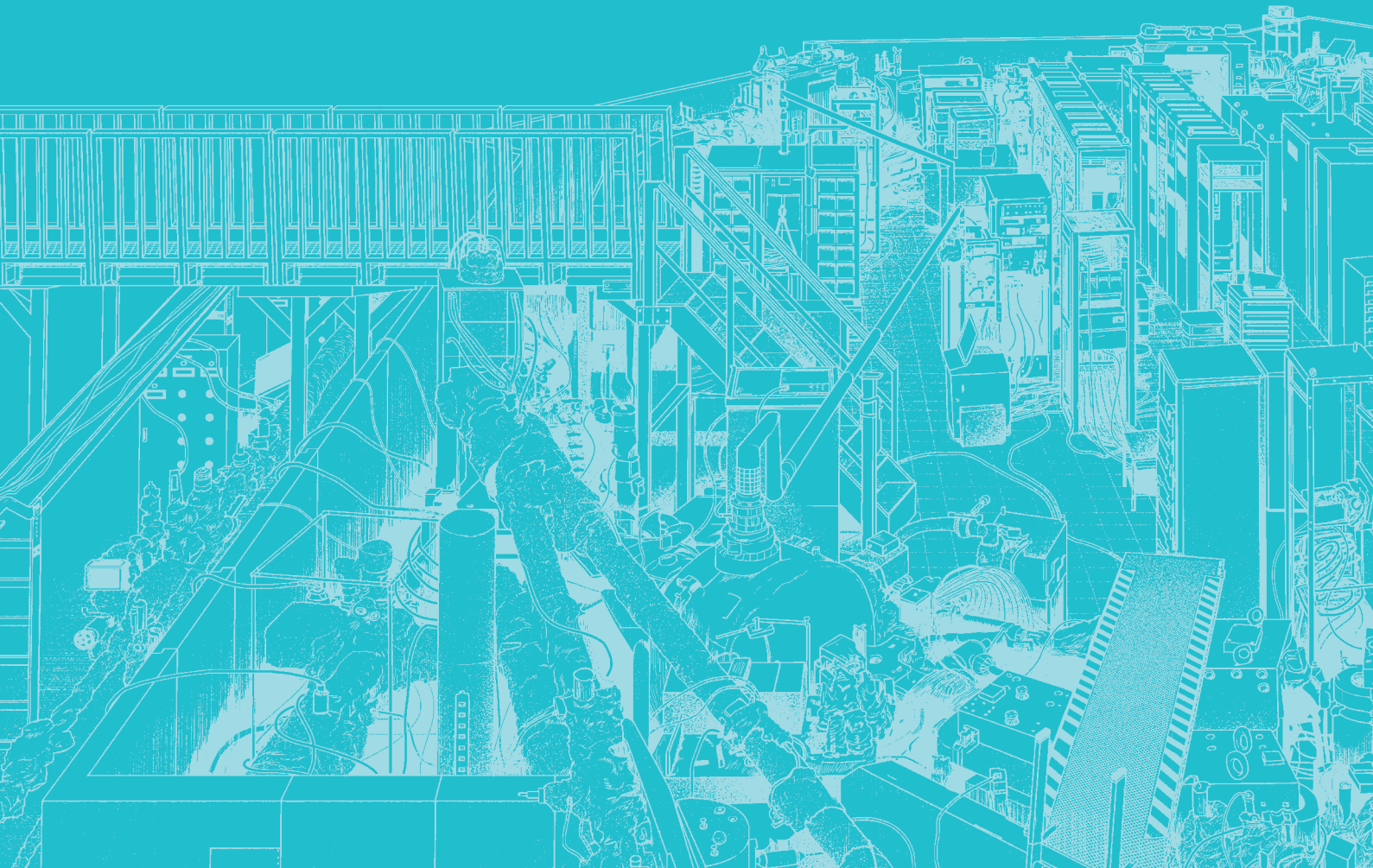


# III-1

Accelerators and  
Instruments





BL1U

## Spectral Phase Interferometry for Direct Electric-field Reconstruction of Undulator Radiation

T. Fuji<sup>1</sup>, T. Kaneyasu<sup>2</sup>, M. Fujimoto<sup>3</sup>, Y. Okano<sup>3</sup>, E. Salehi<sup>3</sup>, M. Hosaka<sup>4,5</sup>, Y. Takashima<sup>4</sup>,  
A. Mano<sup>4</sup>, Y. Hikosaka<sup>6</sup>, S. Wada<sup>7</sup> and M. Katoh<sup>8,3</sup>

<sup>1</sup>Laser Science Laboratory, Toyota Technological Institute, Nagoya 468-8511, Japan

<sup>2</sup>SAGA Light Source, Tosu 841-0005, Japan

<sup>3</sup>Institute for Molecular Science, Okazaki 444-8585, Japan

<sup>4</sup>Synchrotron Radiation Research Center, Nagoya University, Nagoya, 464-0814, Japan

<sup>5</sup>National Synchrotron Radiation Laboratory, University of Science and Technology of China, Hefei 230029, China

<sup>6</sup>Institute of Liberal Arts and Sciences, University of Toyama, Toyama 930-0194, Japan

<sup>7</sup>Graduate School of Advanced Science and Engineering, Hiroshima University, Higashi-Hiroshima 739-8526, Japan

<sup>8</sup>Hiroshima Synchrotron Radiation Center, Hiroshima University, Higashi-Hiroshima 739-0046, Japan

An undulator is a device widely used in modern synchrotron light sources to produce quasi-monochromatic light. The waveform of the electric field produced by a relativistic electron in the undulator is primarily determined by the number of magnets and the gap between them. Although a simple electromagnetic theory predicts a square-shaped waveform, it has never been measured due to the lack of a suggested method. Therefore, it is crucial to characterize the electric field produced by the undulator for the development of synchrotron sources.

SPIDER is a femtosecond pulse characterization method that has been widely used since its invention in 1998 [1]. It involves retrieving the spectral phase by analyzing the fringes of the interferogram between a test pulse and a spectrally sheared replica. At the UVSOR-III synchrotron light source, a tandem undulator produces two wave packets whose wavelengths can be individually adjusted by changing the gap between the permanent magnets of each undulator. A phase shifter consisting of three pairs of electromagnets forms a small chicane for the electron beam and controls the delay between the wave packets in the femtosecond regime with attosecond accuracy.

The twin tandem undulator produces a pair of wavelength-shifted wave packets with a delay, and the interferogram between them can be regarded as a “SPIDER” interferogram. Consequently, we can use the same algorithm as SPIDER to analyze the interferogram and reconstruct the electric field generated by the undulator [2].

The experiment took place at the 750-MeV UVSOR-III storage ring, where a tandem undulator was installed as shown in Figure 1. The undulator consisted of twin APPLE-II type variable polarization devices that operated in the horizontal linear polarization mode, with 10 magnetic periods and a period length of 88 mm. The central photon energy of the fundamental radiation

was adjusted to 35 eV. Figure 2 displays the retrieved electric field, which shows 10-cycle field oscillations with a rectangular envelope of the wave packet that are accurately reproduced.

This method is advantageous for shorter wavelength synchrotron radiation, including soft and hard x-rays, as it does not require nonlinear wavelength conversion. Additionally, it holds potential for the characterization of FEL pulses.

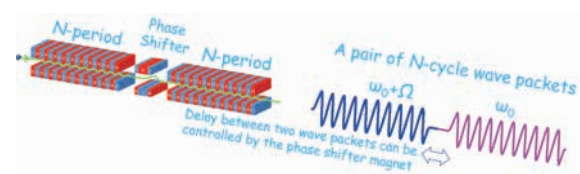


Fig. 1. Conceptual diagram of the tandem undulator.  $\omega_0$  and  $\omega_0 + \Omega$  represent the carrier frequencies of the upstream and downstream wave packets, respectively.

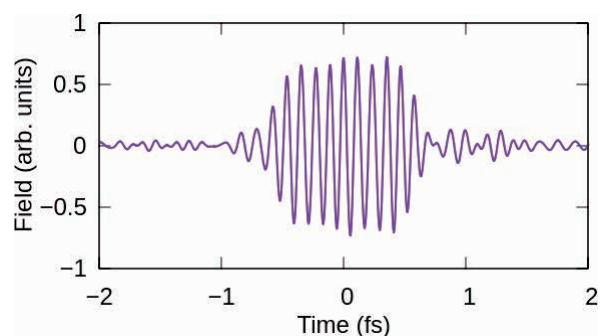


Fig. 2. Waveform of the wave packet retrieved using the SPIDER algorithm.

[1] C. Iaconis and I. A. Walmsley, *Opt. Lett.* **23** (1998) 792.

[2] T. Fuji *et al.*, *Optica* **10** (2) (2023) 302.

## Construction of Laser Transport Line and Light Measurement Setup for Coherent Harmonic Generation Experiment at BL1U

F. Sakamoto<sup>1</sup>, H. Zen<sup>2</sup>, T. Tanikawa<sup>3</sup>, Y. Taira<sup>4</sup>, Y. Okano<sup>4</sup>, H. Ohta<sup>4</sup>,  
J. Yamazaki<sup>4</sup>, K. Hayashi<sup>4</sup>, Y. Takashima<sup>5</sup>, A. Mano<sup>5</sup> and M. Katoh<sup>4,6</sup>

<sup>1</sup>National Institute of Technology, Akita College, Akita 011-8511, Japan

<sup>2</sup>Institute of Advanced Energy, Kyoto University, Kyoto 611-0011, Japan

<sup>3</sup>Innovation Center for Applied Superconducting Accelerators (iCASA), High Energy Accelerator Research Organization (KEK) Ibaraki 305-0801, Japan

<sup>4</sup>UVSOR Synchrotron Facility, Institute for Molecular Science, Okazaki 444-8585, Japan

<sup>5</sup>Synchrotron Radiation Research Center, Nagoya University, Nagoya 464-8603, Japan

<sup>6</sup>HiSOR, Hiroshima University, Higashi-Hiroshima 739-0046, Japan

Coherent Harmonic Generation (CHG) is a method to imprint external laser information to an electron beam and generate temporally coherent and short VUV radiations from it [1]. Since the properties of the CHG such as polarization, temporal and spectral distribution are completely dependent on the external laser [2], they can be optimized by changing the laser and electron beam conditions. These features of the CHG have possibilities for some applied experiments. So far, some experiments on CHG have been performed at UVSOR-II and important features of CHG were observed [3, 4].

We plan to resume detailed studies of CHG using an optical klystron and an ultrashort Ti:Sapphire laser pulse at BL1U. The optical klystron of BL1U consists of two APPLE-II variable polarization undulators and a buncher magnet which is located between the undulators [5]. The laser pulse is injected into the first undulator and an energy exchange between the laser pulse and electron beam that circulates in the storage ring occurs. This leads to an energy modulation inside the electron beam. In the buncher magnet, the energy modulation is converted to a density modulation with a period of the laser wavelength (micro-bunching). Temporally coherent radiations are generated from the micro-bunched electrons in the second undulator.

In order to perform the CHG experiment, we have newly constructed a laser transport line and light measurement setup at BL1U. Schematics of the setup are shown in Fig. 1. The laser pulse is transported about 10 m from laser hutch and injected to the vacuum tube connected to the storage ring. The polarization state is controlled by a  $\lambda/2$  waveplate and a polarization beam splitter (PBS). We also set a monitoring system to adjust spatial and temporal overlaps between the laser and electron beam using CMOS and streak cameras. After the construction of the setup, we have performed the first CHG experiment at BL1U.

The experiment was performed with an electron beam energy of 600 MeV. A resonant wavelength of the undulators was set to 800 nm which corresponds to the wavelength of Ti:Sapphire laser. Figure 2 shows the streak camera images. From these images, we can confirm the laser pulse of 1 ps was well overlapped on the undulator radiation (i.e., electron beam) of 100 ps.

We also observed the spatial overlap by using CMOS camera that was focused in the first undulator. The first target wavelength for the observation was set to 267 nm which was 3rd harmonics of the radiation from the micro-bunching. For the purpose, CHG and Ti:Sapphire pulses were separated by using a dichroic mirror and a band pass filter (BPF) at a downstream of undulators. A photo-multiplier tube (PMT) was used to monitor an intensity of the CHG signals but unfortunately no CHG signals was observed. We are considering the spatial overlap between the laser pulse and electron beam in the first undulator was not good enough. For the next experiment, we plan to remodel the alignment optics for the spatial overlap.

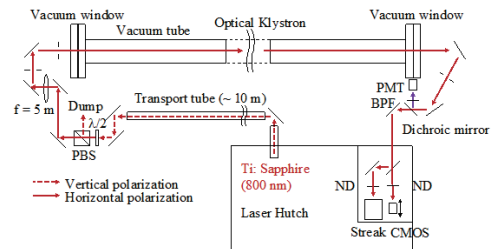


Fig. 1. Schematics of laser transport line and light measurement setup.

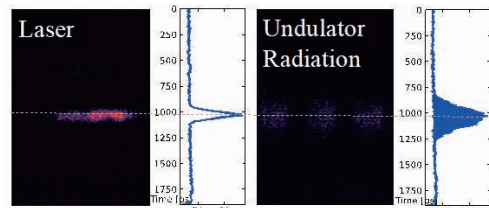


Fig. 2. Streak camera images of laser pulse and undulator radiation. The vertical scale corresponds between right and left images and is synchronized with RF signal of accelerator.

[1] G. Vingola *et al.*, Nucl. Instrum. Methods Phys. Res., Sect. A **239** (1985) 43.

[2] H. Zen *et al.*, Proc. FEL2010 TUPB16 (2010) 286.

[3] M. Labat *et al.*, Eur. Phys. J. D **44** (2007) 187.

[4] T. Tanikawa *et al.*, Appl. Phys. Express **3** (2010) 122702.

[5] Y. Uematsu *et al.*, Proc. PASJ 2012 WEPS066 (2012) 551.

BLIU

## Impact of the Temperature on the Non-Destructive Nuclide Assay in the Transmission NRF Method

M. Omer<sup>1</sup>, T. Shizuma<sup>2</sup>, M. Koizumi<sup>1</sup>, Y. Taira<sup>3</sup>, H. Zen<sup>4</sup>, H. Ohgaki<sup>4</sup> and R. Hajima<sup>2</sup>

<sup>1</sup>Japan Atomic Energy Agency, Tokai 319-1195, Japan

<sup>2</sup>National Institutes for Quantum Science and Technology, Kizugawa 619-0215, Japan

<sup>3</sup>UVSOR Synchrotron Facility, Institute for Molecular Science, Okazaki 444-8585, Japan

<sup>4</sup>Institute of Advanced energy, Kyoto University, Uji 611-0011, Japan

Nuclear resonance fluorescence (NRF) is the photoexcitation of a nuclide using high energy  $\gamma$ -rays. The resonating levels excited by NRF are a fingerprint of each nucleus. Therefore, NRF can be employed as a non-destructive assay technique for nuclear materials such as fissile isotopes. There are two schemes for NRF measurement. The first one is scattering NRF measurement, by which the sample is irradiated by a  $\gamma$ -ray beam, and the scattered NRF photons are measured. The second scheme is the transmission NRF measurement, by which the absorption of NRF photons by the sample is measured. To realize absorption measurement, a second target (witness target of the same sample located downstream the sample target) is used to estimate the amount of  $\gamma$ -ray absorption in the sample. In transmission NRF,  $\gamma$ -ray detector is positioned close to the witness target. So, the measurement is possible without the shadow of background radiation from the sample target. [1].

The emission and absorption rate of NRF  $\gamma$ -rays depend on the temperature of the scattering and witness targets via the Doppler broadened widths of NRF levels. Therefore, the temperature of the scattering and witness targets may affect the time and sensitivity of the measurement. Based on the level widths, many isotopes are possible candidates to study the effect of temperature on transmission NRF, such as <sup>27</sup>Al, <sup>48</sup>Ti, <sup>51</sup>V, <sup>206</sup>Pb, and <sup>208</sup>Pb. In the present measurement, <sup>208</sup>Pb target was irradiated with laser Compton scattering (LCS)  $\gamma$ -ray beam at BLIU of UVSOR. LCS  $\gamma$ -rays of maximum energy of 5.54 MeV were produced from the collision of 746-MeV electrons with laser photons of a wavelength of 1.98  $\mu$ m. A lead collimator with 20-cm thickness and 3-mm aperture size was used to confine the generated  $\gamma$ -rays energy width to approximately 8% (FWHM). Three 140% HPGe detectors, located horizontally, were used to detect NRF  $\gamma$ -rays. Two of them were positioned at a scattering angle of 135° and the third at a scattering angle of 70° with respect to the incident  $\gamma$ -ray direction, as shown in Fig. 1.

A typical  $\gamma$ -ray spectrum measured using <sup>208</sup>Pb is shown in Fig. 2. NRF peaks of <sup>208</sup>Pb were observed as indicated in Fig. 2. We also observed substantial background lines at energies higher than the maximum energy of the LCS  $\gamma$ -ray beam. These lines probably originate from the neutron capture interactions with materials surrounding the experimental setup. The

neutron capture background affects the accuracy of NRF peaks. We applied a 10-cm thickness lead shield around one detector to decrease the background. As shown in Fig. 2 (green spectrum), the background was effectively suppressed. The shielding configuration will be applied in the planned transmission NRF experiments. This work is a contribution of the JAEA to the International Atomic Energy Agency (IAEA) under the agreement of the coordinated research program (CRP), J02015 (Facilitation of Safe and Secure Trade Using Nuclear Detection Technology - Detection of RN and Other Contraband).



Fig. 1. Photo of the experimental setup used for the cryo-NRF experiment at BLIU.

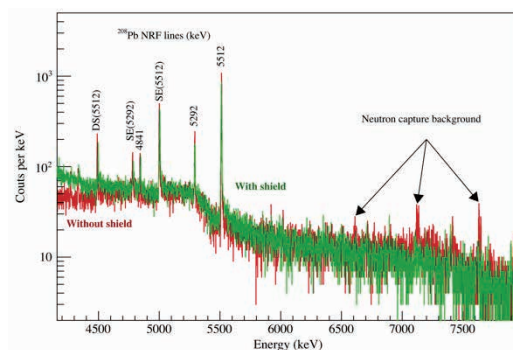


Fig. 2. Typical  $\gamma$ -ray spectra observed for <sup>208</sup>Pb before (red) and after (green) heavy shield. NRF levels are labeled with resonance energies. Also, single and double escape peaks are labeled. The high energy background was effectively suppressed.

[1] C.T. Angell *et al.*, Nucl. Instrum. Methods Phys. Res. B **347** (2016) 11.

## Basic Study on Compton Camera for Detection of Polarized gamma-rays

K. Shimazoe<sup>1</sup>, M. Uenomachi<sup>2</sup>, T. Ueki<sup>1</sup>, Q. Shu<sup>1</sup>, A. Takeda<sup>3</sup>, K. Magata<sup>3</sup>,  
K. Nagayanagi<sup>3</sup> and Y. Taira<sup>4</sup>

<sup>1</sup>Graduate School of Engineering, The University of Tokyo, Tokyo 113-8656, Japan

<sup>2</sup>Space Unit, Kyoto University, Kyoto 606-8502, Japan

<sup>3</sup>Miyazaki University, Miyazaki 889-2192, Japan

<sup>4</sup>UVSOR Synchrotron Facility, Institute for Molecular Science, Okazaki 444-8585, Japan

Compton imaging is a promising technology visualizing the distribution of gamma-rays by using the Compton kinetics principle. Measuring the energies in scatterer and absorber determines the scattering angle of gamma-rays and enables the localization of radiation source. Compton imaging is now widely investigated for the application of astronomy, medical imaging [1] and environmental monitoring [2]. Although the gamma-ray imaging is possible through Compton imaging, but the information of polarization in gamma-ray is not well utilized till now. The polarization information can be used to improve the image quality in positron emission tomography (PET) scanners with its quantum entanglement nature [3].

In the previous research, we have been working on developing silicon on insulator (SOI) based monolithic sensor integrating the silicon sensor and readout electronics in one chip [4]. SOI device can be used to detect the track of Compton recoil electrons for the advanced Compton imaging. In this research we investigated the possibility of extracting the polarization information of incoming linearly or circularly polarized gamma-rays through the pattern of electron tracks and Compton scattering angles.

Figure 1 shows the experimental setup for detecting the polarization of gamma-rays. Two SOI pixel sensor are used as scatterers and Compton electron trackers. Eight 8×8 GAGG arrays (pixel size is 3.2 mm and thickness is 9 mm) coupled with SiPM array are used as absorber. All the detectors are synchronized for detecting the coincidence events between detectors.

Figure 2 shows the picture of detector setup aligned to the beam. In this setup 31-47 degree and 45-61 degree scattering events can be acquired for SOI1/GAGG and SOI2/GAGG coincidence respectively.

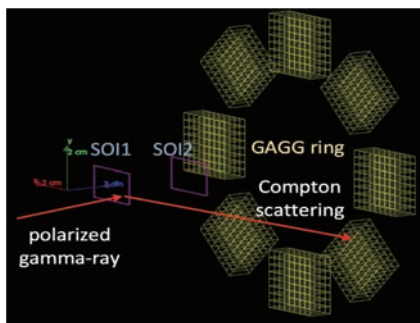


Fig. 1. Two SOI sensors and eight GAGG arrays are used to detect polarized gamma-rays.

Figure 3 shows the expected scattering angle of polarized photon with a Monte Carlo simulation code (GEANT4).

In the first analysis, the coincidence events are successfully acquired between laser trigger and SOI and between laser trigger and GAGG as shown in Figure 4. The more detail analysis is ongoing.

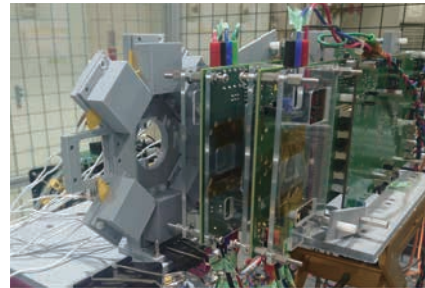


Fig. 2. the detector setup in the beamline BLIU

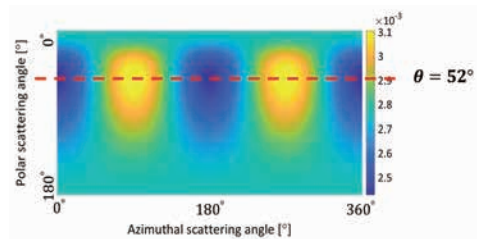


Fig. 3. Simulated scattering angle of polarized photon

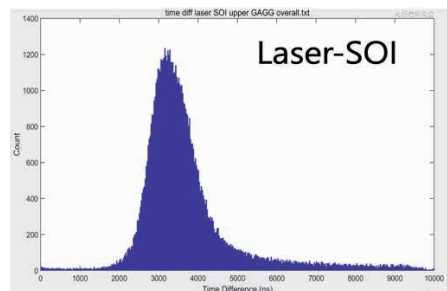


Fig. 4. time difference histogram of SOI and laser

[1] M. Uenomachi, M. Takahashi, K. Shimazoe, *et al.*, *Sci Rep* **11** (2021) 17933 .

[2] Jianyong Jiang, *et al.*, *Journal of Nuclear Science and Technology* **53.7** (2016) 1067.

[3] D. P. Watts, *et al.*, *Nature Communications* **12.1** (2021) 2646.

[4] Y. Yoshihara, *et al.*, *Journal of Instrumentation* **12.01** (2017) C01045.

BLIU

## Development of gamma-ray-induced Positron age-momentum Correlation

Y. Taira<sup>1,2</sup>, Y. Okano<sup>1</sup> and T. Hirade<sup>3</sup>

<sup>1</sup>UVSOR Synchrotron Facility, Institute for Molecular Science, Okazaki 444-8585, Japan

<sup>2</sup>School of Physical Sciences, The Graduate University for Advanced Studies (SOKENDAI), Okazaki 444-8585, Japan

<sup>3</sup>Nuclear Science and Engineering Center, Japan Atomic Energy Agency, Tokai, 319-1195, Japan

In UVSOR-III, gamma-ray-induced positron annihilation spectroscopy using the ultra-short pulsed gamma rays is developed. The ultra-short pulsed gamma rays with a pulse width of ps range are generated via inverse Thomson scattering with 90 degree collisions between an electron beam and a laser pulse at BLIU [1]. Gamma-ray-induced positron annihilation lifetime spectroscopy (GiPALS) is currently available to users. In addition to GiPALS, gamma-ray-induced age-momentum correlation (GiAMOC) is being developed. GiAMOC is an approach to measure the emission time and the energy shift of annihilation gamma rays with an energy of 0.511 MeV simultaneously for observing the time-resolved momentum distribution of an electron, which is the annihilation counterpart of a positron. For that, one of the two annihilation gamma rays produced from a sample is detected using a barium fluoride ( $\text{BaF}_2$ ) detector with high time resolution and the other is detected by a high purity germanium detector (Mirion Technologies, GC4018, 40% relative efficiency) with high-energy resolution. A  $\text{BaF}_2$  detector comprises a  $\text{BaF}_2$  scintillator and a photomultiplier tube (Hamamatsu Photonics K.K., H3378-51). GiAMOC using one detector pair was presented in Ref. [2]. In this report, we present the results of quartz measurements using two detector pairs.

The GiAMOC measurement system is shown in Figure 2 of Ref. [2]. Two sets of this system were used to improve the counting rate by a factor of two, as shown in the picture in Fig. 1. The measured time evolution of a fraction of low-momentum annihilation ( $S$ -parameter) of synthetic silica glass (Tosoh SGM Corp., ED-C) is shown in Fig. 2. As shown in Fig. 2,  $S$ -parameter decreased with time. Around time 0, the annihilation process of para-positronium, which has a short annihilation lifetime and a small energy spread, is dominant, and as time passes, the annihilation processes of free positrons and ortho-positronium, which have longer lifetimes and larger energy spreads than the para-positronium, is dominant. The time evolution of the measured  $S$ -parameter is consistent with that measured using a slow positron beam at AIST [3].

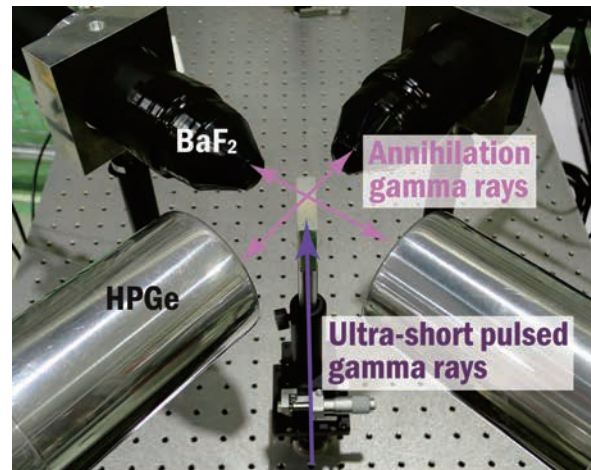


Fig. 1. Detector arrangement of GiAMOC.

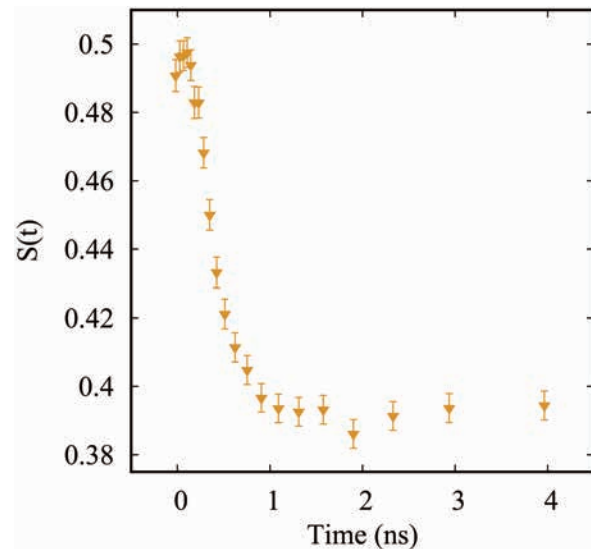


Fig. 2. The time evolution of  $S$ -parameter for synthetic silica glass.

[1] Y. Taira *et al.*, Nucl. Instr. Meth. A **652** (2022) 696.

[2] Y. Taira *et al.*, Rev. Sci. Instr. **93** (2022) 113304.

[3] Y. Komuro *et al.*, Rad. Phys. Chem. **76** (2007) 330.

## Study on Generation of F-LCS Gamma-rays for Absolute Cross-section Measurement of NRF using BL1U Undulator

H. Ohgaki<sup>1</sup>, H. Zen<sup>1</sup>, T. Kii<sup>1</sup>, T. Hayakawa<sup>2</sup>, T. Shizuma<sup>2</sup>, M. Fujimoto<sup>3</sup> and Y. Taira<sup>3</sup>

<sup>1</sup>Institute of Advanced Energy, Kyoto University, Kyoto 611-0011, Japan

<sup>2</sup>Tokai Quantum Beam Science Center, National Institutes for Quantum and Radiological Science and Technology, Ibaraki 319-1106, Japan

<sup>3</sup>UVSOR Synchrotron Facility, Institute for Molecular Science, Okazaki 444-8585, Japan

Laser Compton Scattering Gamma-ray beam (F-LCS), which has a flat distribution in the energy spectrum and the spatial distribution with a few mm diameter beam size, has been developed to study an isotope selective CT Imaging application in the beamline BL1U in UVSOR. By using a circular motion of the electron beam which is excited by a helical undulator installed in a storage ring, and collision with an intense laser beam, an F-LCS beam can be generated. The principle is that the electron beam divergence could be enlarged by the undulator field that enlarges the beam divergence of the Compton backscattered gamma-ray (LCS) beam. At the same time, the LCS beam energy is also spread.

An Electron Gamma Shower version 5 (EGS5) [1] simulation study assumed in the LCS beamline BL1U (Fig.1) with the collimator diameter of 2 mm  $\phi$ . has been carried out. Figure 2 shows the energy spectra of the LCS beams with K-values from 0 to 0.4. The boarder energy spread peak is observed with a larger K-value. The energy spread is widened from 2.7 to 22% (FWHM), and the peak energy is shifted from 5.53 MeV to 5.01 MeV by increment of the K-value from 0 to 0.4. On the other hand, the F-LCS beam yield at the top energy region decreases with the increase of the undulator field. Therefore, K-value of 0.2 could be recommended for practical applications in BL1U.

A POP experiment was carried out at the BL1U in UVSOR. The experimental setup was the same as that shown in Fig. 2 except for a high-purity germanium (Ge) detector with a relative efficiency of 120% was added after the 2-mm $\phi$  collimator. The stored electron with an energy of 746 MeV and a current of about 6 mA was used. The laser beam from a Tm-fiber laser system (TLR-50-AC-Y14, IPG Laser GmbH) whose wavelength was 1.896  $\mu\text{m}$  with random polarization was used at around 1 W CW power. The spectra of the LCS beams were measured for different K-values from K=0 to 0.3. Although the Ge detector response made complicated energy spectra, we observed peak the shift toward lower energy according to larger K value, as shown in Fig. 3.

As a result, the larger K-value, the broader energy bandwidth of the LCS was observed as predicted by EGS5 simulation. This result supports the successful generation of the F-LCS beam.

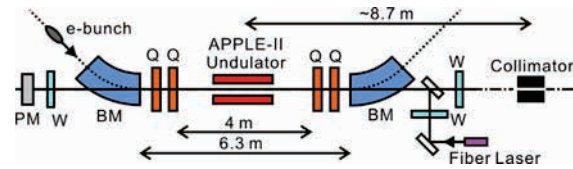


Fig. 1. Schematic drawing of the LCS beamline BL1U, UVSOR. PM: power meter, W: window, SM: Spherical Mirror. A Ge detector was added after the collimator in the POP experiment.

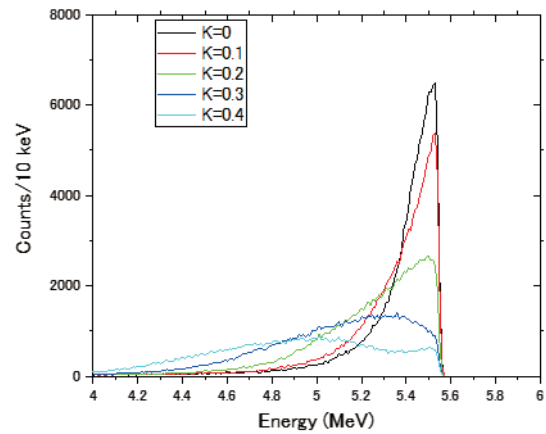


Fig. 2. LCS gamma-ray energy distribution in the vertical axis with the undulator K-value of K=0.2.

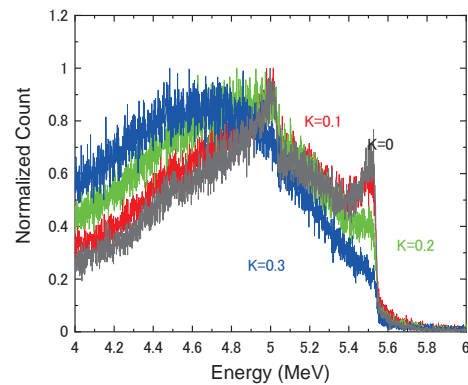


Fig. 3. Measured LCS beam spectra with the undulator K-value of 0, 0.1, 0.2, and 0.3.

[1] H. Hirayama, Y. Namito, A.F. Bielajew, S.J. Wilderman and W.R. Nelson, The EGS5 code system, SLAC Report number: SLAC-R-730, KEK report number: 2005-8 (2005).

BL1U

## Double-Pulsed Light Wave Packets Emitted from a Tandem Undulator

T. Kaneyasu<sup>1,2</sup>, M. Hosaka<sup>3,4</sup>, A. Mano<sup>4</sup>, Y. Takashima<sup>4</sup>, M. Fujimoto<sup>2,4</sup>, E. Salehi<sup>2</sup>,  
H. Iwayama<sup>2,5</sup>, Y. Hikosaka<sup>6</sup> and M. Katoh<sup>2,4,7</sup>

<sup>1</sup>SAGA Light Source, Tosu 841-0005, Japan

<sup>2</sup>Institute for Molecular Science, Okazaki 444-8585, Japan

<sup>3</sup>University of Science and Technology of China, Hefei 230029, China

<sup>4</sup>Synchrotron Radiation Research Center, Nagoya University, Nagoya, 464-8603, Japan

<sup>5</sup>Sokendai (The Graduate University for Advanced Studies), Okazaki 444-8585, Japan

<sup>6</sup>Institute of Liberal Arts and Sciences, University of Toyama, Toyama 930-0194, Japan

<sup>7</sup>Hiroshima Synchrotron Radiation Center, Hiroshima University, Higashi-Hiroshima 739-0046, Japan

The waveform of electromagnetic radiation from an ultra-relativistic electron reflects the motion of the electron. We report on a fully-optical characterization of double-pulsed wave packets emitted by individual relativistic electrons passing through a tandem undulator in a synchrotron light source [1]. The experiment was carried out at the undulator beamline BL1U. The light source of BL1U consists of two identical APPLE-II undulators, between which a three-pole electromagnetic phase shifter is installed (Fig. 1). The period length and number of periods for each undulator were 88 mm and 10, respectively. A relativistic electron passing through the undulators emits a wave packet with a waveform expected to be characterized by time-separated 10-cycle oscillations. The time delay between the double-pulsed components can be controlled by adjusting the length of electron orbit between the undulators using the phase shifter magnet.

Using a Mach-Zehnder interferometer [2] operating at ultraviolet wavelengths, we measured the autocorrelation trace for the spontaneous radiation from the tandem undulator. The double-pulsed wave packets were randomly distributed within the overall 300 ps radiation pulse corresponding to the length of the electron bunch. Figure 2(a) shows the interferograms obtained by setting the field strength of the phase shifter magnet to four different values. The central wavelength of the radiation was 357 nm for both undulators. The interferograms measured at a phase shifter current of 10.0 A or more show approximately 20-cycle oscillations with triangular envelopes in the range of  $-12 - +12$  fs, as well as weaker 20-cycle oscillations lying on both sides. The side oscillation structures approach the central structure as the phase shifter current decreases, and they are unified at a phase shifter current of 0 A.

The observed interferograms can be understood as autocorrelation traces of double-pulsed wave packet. The calculated autocorrelation traces for a double-pulsed 10-cycle sinusoidal wave packet at 357 nm wavelength are shown in Fig. 2(b). Over the whole range of phase shifter currents, one finds excellent agreement between the experiments and calculations.

This fact confirms that each of the relativistic electron emits a double-pulsed 10-cycle wave packet which well reflects the magnetic field in the tandem undulator.

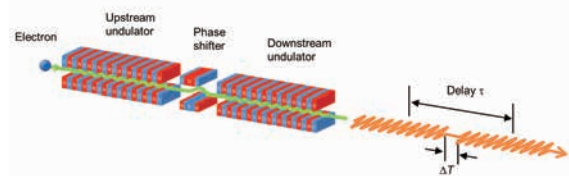


Fig. 1. Schematic illustration of the tandem undulator. A relativistic electron passing through the undulators emits a wave packet with a waveform expected to be characterized by time-separated 10-cycle oscillations.

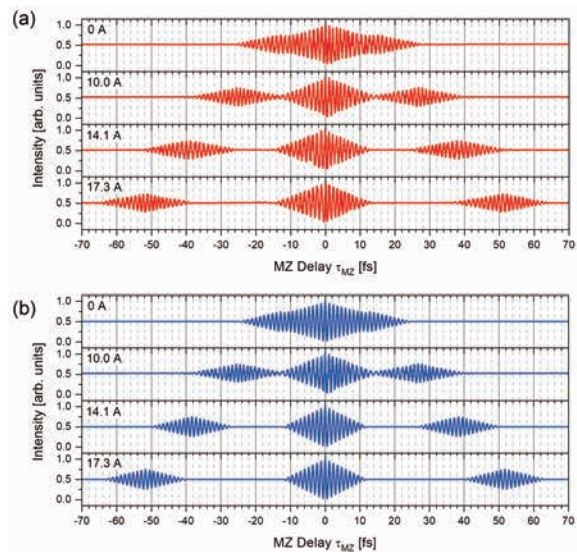


Fig. 2. Autocorrelation measurements of spontaneous radiation from the tandem undulator at various values of the phase shifter current. The wavelength of the fundamental undulator radiation was set to 357 nm. (a) Measurement. (b) Calculation.

[1] T. Kaneyasu *et al.*, *Sci. Rep.* **12** (2022) 9.

[2] A. Mano *et al.*, *UVSOR Activity Report 2020*, **48** (2020) 38.

## Progress in Single Electron Storage Experiment

A. Asai<sup>1</sup>, M. Shimada<sup>2,3</sup>, H. Miyauchi<sup>2,3</sup> and M. Katoh<sup>3,1,4,2</sup>

<sup>1</sup>School of Science, Hiroshima University, Higashi-hiroshima 444-8585, Japan

<sup>2</sup>High Energy Accelerator Research Organization (KEK), Tsukuba 305-0801, Japan

<sup>3</sup>Hiroshima Synchrotron Radiation Research Center, Hiroshima University, Higashi-hiroshima 739-0046, Japan

<sup>4</sup>UVSOR Synchrotron Facility, Institute for Molecular Science, Okazaki 444-8585, Japan

Single electron storage has been achieved at several electron synchrotrons, aiming to investigate electron dynamics in a synchrotron [1,2,3], to investigate electromagnetic radiation from an electron [4], or to utilize the radiation as a primary standard [5,6,7]. In FY2021, we have started an experimental study on single electron storage at UVSOR-III and successfully demonstrated it [8, 9]. In FY2022, we continued improving the operation technique for the single electron storage and also have started some basic studies on undulator radiation [10]. Here, we report some preliminary results. The final results will be published elsewhere in future.

We have established the following procedure for the single electron storage. First, we accumulate an electron beam with very low current, typically 0.1 mA. Indeed, this current corresponds to one shot of the injector. At this low beam current, we could observe and adjust the optical axis by eye from the undulator at BL1U, which is tuned at 355 nm wavelength. Then, we reduce the beam lifetime to several minutes by using beam scraper. We use a photomultiplier tube (PMT) to measure the synchrotron radiation intensity. The PMT signal was analyzed with a counting unit and recorded by a PC. Single electron storage corresponds to about 1 pA beam current. Therefore, we have to observe very wide range of the intensity for many orders of magnitudes. Therefore, we set ND filters in front of the PMT to adjust the radiation intensity and remove them as the intensity reduces. To make the operation simpler, we examined an ultra-wide range PMT and obtained a good result. The details will be described elsewhere in future.

We could observe step function like changes in the intensity as shown in Figure 1, which corresponds to a loss of one electron. We also observed the timing of the PMT output relative to the revolution signal provided by the RF system, as also shown in Figure 1. We could observe in which RF bucket the electrons exists. We confirmed that the last electron survives for more than 2 hours after we pulled out the beam scraper to the original position. This allows us to observe some basic properties of synchrotron radiation. An example is presented in Figure 2, which shows that the photon statistics is well represented by Poisson distribution. Other interesting results will be presented somewhere in future.

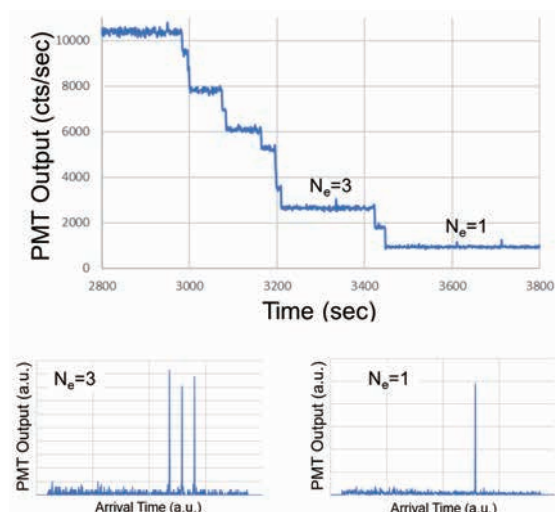


Fig. 1. Synchrotron radiation intensity

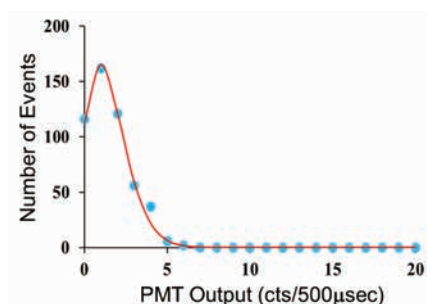


Fig. 2. Photon Statistics observed at BL1U

- [1] A. N. Aleshaev *et al.*, NIM A **359** (1995) 80.
- [2] I. V. Pinayev *et al.*, NIM A **375** (1996) 71.
- [3] A. Romanov *et al.*, 2021 JINST **16** (2021) P12009.
- [4] I. V. Pinayev *et al.*, NIM A **341** (1994) 17.
- [5] R. Klein *et al.*, Phys. Rev. STAB **11** (2008) 110701.
- [6] R. Klein *et al.*, 2010 Metrologia **47** (2010) R33.
- [7] T. Saito *et al.*, Bulletin of the Electrotechnical Laboratory (in Japanese) (1985) 431.
- [8] R. Shinomiya *et al.*, UVSOR Activity Report 2021, (2022) 39.
- [9] R. Shinomiya, Bachelor Thesis (Hiroshima University) (in Japanese) (2022).
- [10] Y. Asai, Bachelor Thesis (Hiroshima University) (in Japanese) (2023).

BL2A

## Calibration of the Soft X-ray Response Matrix of CMOS Detector Used in Sounding Rocket Experiment FOXSI-3

N. Narukage<sup>1,2</sup>, R. Shimizu<sup>2,3</sup>, Y. Sato<sup>1,2</sup> and S. Kashima<sup>3</sup>

<sup>1</sup>National Astronomical Observatory of Japan (NAOJ), Mitaka, 181-8588, Tokyo, Japan

<sup>2</sup>The Graduate University for Advanced Studies, SOKENDAI, Hayama, 240-0193, Kanagawa, Japan

<sup>3</sup>Institute of Space and Astronautical Science (ISAS), Japan Aerospace Exploration Agency (JAXA), Sagami-hara, 252-5210, Kanagawa, Japan

The solar corona is full of dynamic phenomena such as solar flares. The understandings of these phenomena have been progressing step-by-step with the evolution of the observation technology in EUV and X-rays from the space. But there are fundamental questions remain unanswered or haven't even addressed so far. Our scientific objective is to understand underlying physics of the dynamic phenomena in the solar corona, covering some of the long-standing questions in solar physics such as particle acceleration in flares and coronal heating. To achieve this objective, we identify the imaging spectroscopy (the observations with spatial, temporal and energy resolutions) in the soft X-ray range (from  $\sim 0.5$  keV to  $\sim 10$  keV) is a powerful approach for the detection and analysis of energetic events [1]. This energy range contains many lines emitted from below 1 MK to beyond 10 MK plasmas plus continuum component that reflects the electron temperature.

The soft X-ray imaging spectroscopy is realized with the following method. We take images with a short enough exposure to detect only single X-ray photon in an isolated pixel area with a fine pixel Silicon detector. So, we can measure the energy of the X-ray photons one by one with spatial and temporal resolutions. When we use a high-speed soft X-ray camera that can perform the continuous exposure with a rate of more than several hundred times per second, we can count the photon energy with a rate of several 10 photons / pixel / second. This high-speed exposure is enough to track the time evolution of spectra generated by dynamic phenomena in the solar corona, whose lifetimes are about from several ten seconds to several minutes. For the first imaging spectroscopic observation of the solar corona in soft X-ray range, we launched a NASA's sounding rocket (FOXSI-3) on September 7<sup>th</sup>, 2018 and successfully obtained the unprecedented data [2] using a high-speed X-ray camera [3] with a back-illuminated CMOS detector [4].

Calibration of CMOS detectors is essential for scientific data analysis. For this purpose, a completely monochromatic X-ray light source is needed. In addition, the flux must be adjusted so that individual X-ray photons can be isolated. Therefore, we have developed a mirror-based reflective-type flux reduction system [5].

In this time, using this system, the response of the CMOS detector aboard the FOXSI-3 sounding rocket is

completely calibrated in the energy range of 840 eV to 4500 eV in 20 eV intervals (see Fig. 1).

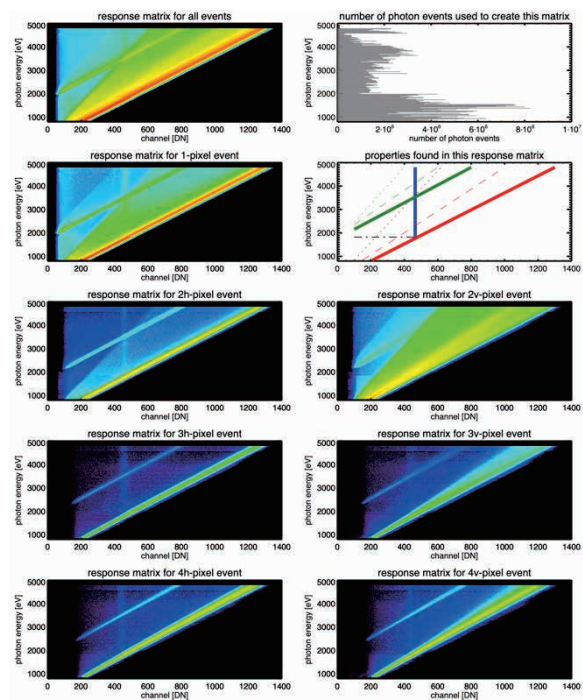


Fig. 1. Measured response matrix of the FOXSI-3 CMOS detector from 840 eV to 4500 eV. In the color maps, the horizontal axis shows the values of output signals from the detector, when the detector detects the monochromatic X-ray photons with the energy shown in the vertical axis. The colors indicate, in log scale, how frequently each signal value is output. The top-right panel shows the number of monochromatic X-ray photons used to create this matrix.

[1] N. Narukage *et al.*, White paper of the “soft X-ray imaging spectroscopy”, arXiv:1706.04536 (2017).

[2] N. Narukage and S. Ishikawa, *UVSOR Activity Report 2018* **46** (2018) 36.

[3] S. Ishikawa *et al.*, *Nucl. Instrum. Methods Phys. Res., Sect. A* **912** (2018) 191.

[4] N. Narukage *et al.*, *Nucl. Instrum. Methods Phys. Res., Sect. A* **950** (2020) 162974.

[5] N. Narukage, *UVSOR Activity Report 2022*, **49** (2021) 42.

## Development of a Transfer Vessel for NEXAFS Spectroscopy

E. Kobayashi<sup>1</sup> and A. Inoishi<sup>2</sup>

<sup>1</sup> *Kyushu Synchrotron Light Research Center, 8-7 Yayoigaoka, Tosu, Saga 841-0005, Japan*

<sup>2</sup> *Institute for Materials Chemistry and Engineering, Kyushu University 6-1 Kasuga-koen, Kasuga-Shi 816-8580, Japan*

Battery materials are contaminated with oxygen, carbon dioxide and water when exposed to the atmosphere. Therefore, we developed a sample transfer vessel that can transport the sample to the analyzer without exposing it to the atmosphere [1, 2]. Furthermore, in order to perform more precise analysis, we developed a transfer vessel with a small ion pump [3]. In recent years, analysis of battery materials using soft X-ray absorption spectroscopy has been performed. However, it was difficult to analyze across the beamline without atmospheric exposure. This is because the sample holders are different depending on the beamline. Therefore, we have developed a transfer vessel that can measure the soft X-ray absorption spectrum across the beamline without exposing the sample to the atmosphere, based on the apparatus that we have developed.

The ZrO<sub>2</sub> powders was attached to the transfer vessel in a glove box under an argon atmosphere. NEXAFS spectra of the ZrO<sub>2</sub> powders using both total electron yield (TEY) and partial fluorescence yield (PFY) modes were measured at the beamline 2A of the UVSOR in the Institute of Molecular Science. For TEY, the drain current of the sample was measured. For PFY, fluorescence X-rays were collected using an energy dispersible silicon drift detector (SDD). All experiments were performed at room temperature.

Fig. 1 shows a photograph of the developed transfer vessel. The sample is fixed to the lower part of the vessel using carbon tape. The sample current is measured using the Bayonet Neill-Concelman (BNC) connector on the upper part of the vessel. Fig. 2 shows the Zr *L*-edge NEXAFS spectra of ZrO<sub>2</sub> powder obtained from TEY and PFY. The shape of the spectrum measured in the TEY mode was almost the same as that measured in the PFY mode. The TEY is surface-sensitive whereas the PFY is sensitive to the bulk. The result indicates that the sample could be transported without air contamination.



Fig. 1. Photograph of the transfer vessel.

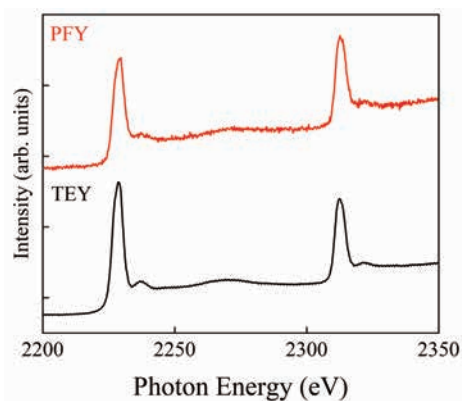


Fig. 2. Zr *L*-edge NEXAFS spectra of ZrO<sub>2</sub> powder obtained from TEY and PFY.

[1] E. Kobayashi, J. Meikaku, T. Okajima, and H. Setoyama, Japanese Patent No. 5234994.

[2] E. Kobayashi, J. Meikaku, H. Setoyama, T. Okajima, *J. Surf. Anal.*, **19** (2012) 2.

[3] E. Kobayashi, S. Tanaka, T. Okajima. *J. Vac. Soc. Jpn.* **59** (2016) 192.

BL3U

## Soft X-ray Transmission Measurements of Polymer Films for Soft X-ray Absorption Spectroscopy of Liquids in Low-Energy Regions

M. Nagasaka<sup>1,2</sup>, S. Fujikawa<sup>3</sup>, H. Takaya<sup>1,4</sup> and Y. Uozumi<sup>1,2</sup>

<sup>1</sup>*Institute for Molecular Science, Okazaki 444-8585, Japan*

<sup>2</sup>*The Graduate University for Advanced Studies (SOKENDAI), Okazaki 444-8585, Japan*

<sup>3</sup>*International Institute for Carbon-Neutral Energy Research (WPI-I2CNER) and Research Center for Negative Emissions Technologies, Kyushu University, 744 Moto-oka, Nishi-ku, Fukuoka 819-0395, Japan*

<sup>4</sup>*Department of Life Science, Faculty of Life & Environmental Sciences, Teikyo University of Science, Main Buld #15-05, 2-2-1 Senjyusakuragi, Adachi-ku, Tokyo 120-0045, Japan*

Soft X-ray absorption spectroscopy (XAS) is an element-specific method to investigate electronic structures of liquids. The soft X-ray regions below 2 keV have chemically and biologically absorption edges such as K-edges of C, N, and O and L-edges of transition metals such as Mn, Fe, Co, and Ni. Recently, we have developed a transmission-type liquid cell, where a liquid layer is sandwiched between two Si<sub>3</sub>N<sub>4</sub> membranes with the thickness of 100 nm, and measured XAS spectra of several liquid samples in transmission mode by adjusting the liquid thicknesses precisely from 20 nm to 2000 nm [1].

The low-energy regions below 200 eV include absorption edges for the investigation of chemical and biological phenomena in solutions such as K-edges of Li and B and L-edges of Si, P, S, and Cl. Since soft X-ray transmission in the low-energy region is extremely lower than that in the high-energy region above 200 eV [2], transmitted soft X-rays below 200 eV include many high-order X-rays. Recently, we have used an argon gas window for removing high-order X-rays by using the Ar L-edge (240 eV) [3] and developed the soft X-ray detector that removes high-order X-rays [4]. However, the XAS measurements in the low-energy regions are still difficult since soft X-rays are strongly absorbed by Si<sub>3</sub>N<sub>4</sub> membranes with the Si L-edges (100 eV). In this study, we have synthesized polymer films that include no Si atoms with the thickness of 100 nm and evaluated the soft X-ray transmission of the polymer film.

The experiments were performed at BL3U. The polymer film was settled under an ultrahigh vacuum condition, which directly connected to the beamline. The transmitted soft X-rays through the polymer film were measured by using a photodiode detector.

Figure 1 shows the soft X-ray transmission of the polymer film in the soft X-ray region from 50 eV to 560 eV. Since the polymer film includes the C=C and C=N groups, the sharp absorption peaks such as the transition from C 1s electrons to C=C  $\pi^*$  orbitals at the C K-edge and the transition from N 1s electrons to C=N  $\pi^*$  orbitals at the N K-edge are observed. Note that the soft X-ray beamline BL3U includes three monochromatic gratings for covering wide photon energy regions. The

photon intensities are also maximized by adjusting the undulator gap. That is why several photon energy regions are not continuous due to the different gratings and the orders of the undulator gap. Since the polymer film includes no Si atoms, there is no peaks at the Si L-edge. Soft X-ray transmission of the polymer film shows a still high value below 200 eV, indicating the present polymer film is suitable to measure XAS of liquids in the low-energy region.

In the present, we have developed an ultrathin liquid cell to reduce the optical pass length of Ar gas. We will include the present polymer films to the ultrathin liquid cell for improving the soft X-ray transmission of liquid samples in the low energy region below 200 eV.

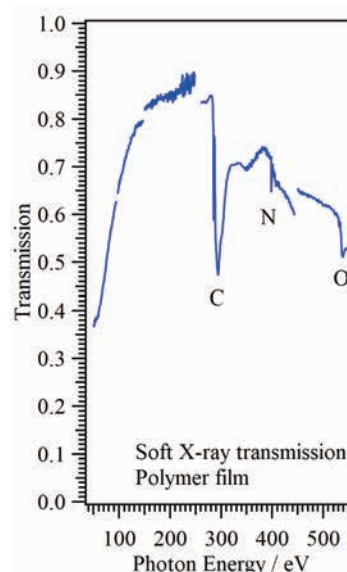


Fig. 1. Soft X-ray transmission of the polymer film.

- [1] M. Nagasaka and N. Kosugi, *Chem. Lett.* **50** (2021) 956.  
 [2] C. T. Chantler, *J. Phys. Chem. Ref. Data* **29** (2000) 597.  
 [3] M. Nagasaka, *J. Synchrotron Rad.* **27** (2020) 959.  
 [4] M. Nagasaka and H. Iwayama, *Rev. Sci. Instrum.* **91** (2020) 083103.

## Dissociation Channels of Molecules for a Use of Plasma Etching Processes

T. T. Nguyen<sup>1</sup>, K. Ishikawa<sup>1</sup> and H. Iwayama<sup>2</sup>

<sup>2</sup>Nagoya University Center for low-temperature plasma sciences, Nagoya 464-8601,

<sup>1</sup>UVSOR Synchrotron Facility, Institute for Molecular Science, Okazaki 444-8585, Japan

Plasma etching is indispensable for the fabrication of semiconductor devices. In recent years, there has been an urgent need to develop etching gases that meet the requirements for manufacturing three-dimensional devices and high aspect ratio structures. For the plasma-etching, hydrofluorocarbon molecules are used. Plasma dissociates and ionizes gas molecules. The plasma-related reactions are complicated significantly, however these reactions of dissociated and ionized fragments of molecules should be controlled on the basis of scientific understanding. First, we predicted dissociation and ionization channels of gas molecules using computational chemistry. As the results, we calculated precisely the excited state of perfluorocarbon, *c*-C<sub>4</sub>F<sub>8</sub> [1]. In order to improve the accuracy of the reaction prediction, experimental verification of photodissociation is required.

In this study, experimental verification of dissociation of perfluorocarbons, which are not in the database for plasma-etching gases, mainly hydrofluorocarbon molecules, has been performed with precision and accuracy using beamlines owned by the Institute for Molecular Science (IMS). Through this study, we will pioneer the future development of the world's best plasma etching gas by combining coincidence spectroscopy and computational chemistry.

This study conducted coincidence spectroscopy experiments on photoionization and photodissociation using vacuum ultraviolet light region from 40 nm to 400 nm from beamlines of BL3B in the IMS. This light source is the only facility in Japan.

In the etching process plasmas, abundances for dissociated ions are reported by C<sub>3</sub>F<sub>5</sub><sup>+</sup> > CF<sub>3</sub><sup>+</sup> > CF<sup>+</sup> > C<sub>2</sub>F<sub>4</sub><sup>+</sup>, which are different C<sub>2</sub>F<sub>4</sub><sup>+</sup> > C<sub>3</sub>F<sub>5</sub><sup>+</sup> > CF<sup>+</sup> > CF<sub>3</sub><sup>+</sup> in mass spectra taken at 70 eV electron energy. The calculation results showed that a secondary process of *c*-C<sub>4</sub>F<sub>8</sub><sup>+</sup> to C<sub>2</sub>F<sub>4</sub> + C<sub>2</sub>F<sub>4</sub><sup>+</sup> dissociation route is a potential barrier of 12.05 eV (Fig. 1, Table 1), which is well corresponded with the calculated energy barrier of 12.0 eV along the C<sub>2</sub>F<sub>4</sub><sup>+</sup> dissociation route [1]. The C<sub>3</sub>F<sub>5</sub><sup>+</sup> ion production channel is the lowest energy barrier due to intramolecular rearrangement reaction, that is *c*-C<sub>4</sub>F<sub>8</sub><sup>+</sup> → C<sub>3</sub>F<sub>5</sub><sup>+</sup> + CF<sub>3</sub> and additionally *c*-C<sub>4</sub>F<sub>8</sub><sup>+</sup> ions C<sub>2</sub>F<sub>4</sub><sup>+</sup> channel is the second lowest energy barrier. The other fragments such as C<sub>3</sub>F<sub>5</sub><sup>+</sup>, CF<sub>3</sub><sup>+</sup>, CF<sup>+</sup>, are produced by intermolecular rearrangement reactions.

Consequently, the ionization process of C<sub>3</sub>F<sub>5</sub><sup>+</sup> channel is abundant due to the lowest potential barrier.

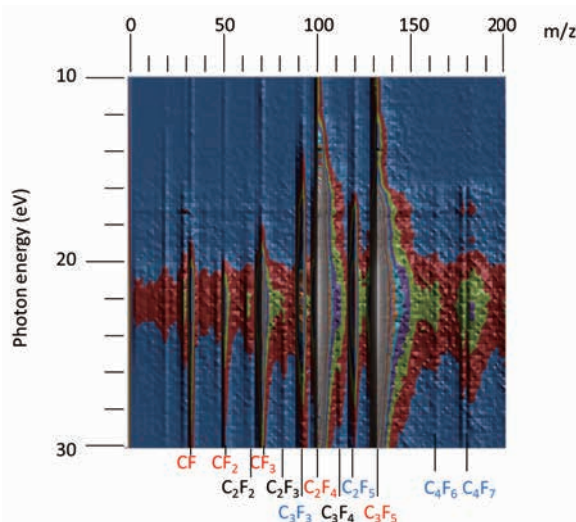


Fig. 1. Typical mass spectral intensities by photoionization of *c*-C<sub>4</sub>F<sub>8</sub> measured vacuum ultraviolet ranges from 10 to 30 eV.

Table 1. Ionization potential (IP) and appearance potentials (AP) for *c*-C<sub>4</sub>F<sub>8</sub>.

	Ions	Potential Calc. [1]	(eV) Exp.	References
IP	<i>c</i> -C <sub>4</sub> F <sub>8</sub> <sup>+</sup>	11.5	<b>11.55</b>	This study
AP	<i>c</i> -C <sub>4</sub> F <sub>7</sub> <sup>+</sup>	15.1	<b>15.45</b>	This study
	C <sub>3</sub> F <sub>5</sub> <sup>+</sup>	12.0	12.1 <b>11.85</b>	Lifshitz[2] This study
	C <sub>2</sub> F <sub>4</sub> <sup>+</sup>	12.4 12.0*	12.35 <b>12.05</b>	Lifshitz[2] This study
	CF <sub>3</sub> <sup>+</sup>	12.5	14.4 <b>16.6</b>	Lifshitz[2] This study
	CF <sub>2</sub> <sup>+</sup>	14.8	17.9	This study
	CF <sup>+</sup>	13.6	18.4 <b>17.1</b>	Lifshitz[2] This study

\* vertical ionization potential

[1] T. Hayashi, *et al.* Jpn. J. Appl. Phys. **61** (2022) 106006.

[2] C. Lifshitz, *et al.* Int. J. Mass Spectrum Ion Phys. **10** (1972) 25.

BL3B

## Study of Luminescence Characteristics of Diamond Scintillator for Dark Matter Search

A. Umemoto

*Division of Physics, University of Tsukuba, Tennoudai, Tsukuba, Ibaraki, 305-8571, Japan*

Direct detection of dark matter is one of the highest priorities in astroparticle physics. The dark matter in Milky Way Galaxy can be detected via elastic scattering from nuclei in a detector on the earth. For the direct dark matter search, diamond is one of the promising detector. The highest Debye temperature among crystals (2200 K) and optical centers due to defects and impurities are unique physical properties of diamond, and they might make good performance of a diamond scintillating bolometer [1][2].

With the goal of developing a diamond scintillating bolometer for dark matter search, we constructed an experimental system to measure a photoluminescence property of synthetic diamond at BL3B in UVSOR. Usually, the measurements at BL3B are conducted by the following setup: the excitation light is incident on a sample surface at an angle of  $45^\circ$ , and fluorescence is detected with a CCD placed at right angles to the excitation light. But this measurement setup will not work well for diamond due to the total internal reflection because the refractive index of diamond ( $n = 2.42$ ) is much larger comparing with that of air (also vacuum). Therefore, a measurement system using a right angle prism as shown in the schematic diagram of Fig.1 was designed. The excitation deviated a light path by  $90^\circ$  by entering one side of the prism will be made incident on the diamond attached on the other side of the prism by vacuum grease. The system makes it possible for the CCD to detect the photoluminescence of diamond emitted in a direction perpendicular to the diamond surface. We used a UV fused silica right angle prism with length of 10 mm manufactured by Thorlabs, which transmits more than 90% of light with wavelengths more than 185 nm.

Fig.2 shows a photoluminescence spectrum of a diamond excited by ultra violet light with wavelength of 200 nm. The diamond is a commercially available synthetic crystal with a size of  $3 \times 3 \times 0.3$  mm manufactured by a method of high-pressure high-temperature. Nitrogen impurities of the diamond is less than 200 ppm. Although a peak due to the second-order diffraction of the excitation light was also observed, the shape of the spectrum detected in the wavelength of

$500 < \lambda < 700$  nm was consistent with our previous result of X-ray radio luminescence spectrum. It was demonstrated that the measurement system is useful for detecting a photoluminescence of diamond. In FY2023, we plan to perform low-temperature measurements with this setup to quantify the luminescence properties of diamond scintillators.

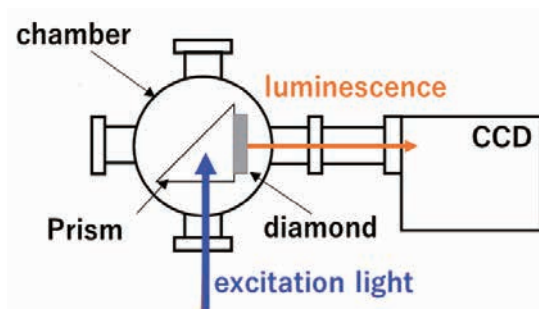


Fig. 1. A design of the experimental setup for photoluminescence measurement of diamond.

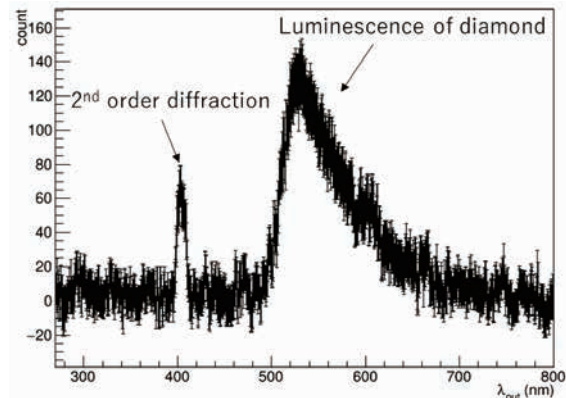


Fig. 2. Photoluminescence spectrum of a commercially available HPHT diamond measured by using the system shown as Fig.1. Ultra violet light with wavelength of 200 nm was used for photoluminescence excitation.

[1] T.L. Nam *et al.*, *Appl. Radiat. Isot.* **40** (1989) 8.

[2] L. Canonica *et al.*, *J. Low. Temp. Phys.* **189** (2020) 606.

## Current Photon Flux and Focus Size of BL4B

H. Iwayama<sup>1,2</sup>

<sup>1</sup>UVSOR Synchrotron Facility, Institute for Molecular Science, Okazaki 444-8585, Japan

<sup>2</sup>School of Physical Sciences, The Graduate University for Advanced Studies (SOKENDAI), Okazaki 444-8585, Japan

Beamline BL4B has three holographically ruled laminar profile plane gratings (G1: 800 lines/mm, G2: 267 lines/mm, G3: 100 lines/mm) and covers soft X-ray regions ranging from 40 eV to 1000 eV. This soft x-ray region includes K-edge energies of light elements such as C, N, and O and L-edge energies of transition metals such as Mn, Fe, and Co. Since an endstation of BL4B is not fixed for specific equipment, users can bring in their equipment and connect them to BL4B. The main experiments at BL4B are X-ray magnetic circular dichroism (XMCD), angular resolved photoemission spectroscopy (ARPES), and X-ray absorption fine structure (XAFS) measurements.

The BL4B uses synchrotron radiation from a bending magnet, and its photon flux and focus size are weak and large compared to undulator beamlines. While BL4B is difficult to measure in tiny samples, it is suitable for organic molecules, which are fragile against radiation damage. Thus photon density is an important parameter for estimating radiation damage on the sample.

This work measured photon flux and focus image at the focus point. We use a photodiode and Ce:YAG scintillator for photo flux and focus image measurements.

Figure 1 shows photon flux curves for each grating. Entrance and exit slits of the beamline are set to 50  $\mu\text{m}$ . The photon flux is almost the same as the previous one measured in 2005, and a photon flux is higher than the previous one for a high photon energy region of more than 400 eV. In 2012, our facility improved the optics of electron storage ring, such as bending magnets, and upgraded from UVSOR-II to UVSOR-III. While electron trajectories in the storage ring were significantly changed after the major update of UVSOR synchrotron, the photon flux curves measured this time indicate that beamline optics were optimized well and the throughput and photon flux of the beamline was maintained.

Figure 2 shows a photo of measurement equipment for a focus image. The equipment comprises Ce:YAG scintillator, ultra-long working distance lens, and CMOS camera. The scintillator is in a vacuum chamber and irradiated by soft X-ray beam of BL4B. The irradiated scintillator emits  $\sim 550$  nm fluorescence, and we observed them by the ultra-long working distance lens and CMOS camera. This lens's working distance and optical magnification are 305 mm and 0.37  $\sim$  4.48, respectively. The highest space resolution is 7  $\mu\text{m}$ .

Figure 3 shows a typical focus image. Photon energy and flux are 400 eV and  $8 \times 10^9$  photons/s. An exposure

time is 30 seconds. This image exhibits a focus size of  $\phi \sim 500$   $\mu\text{m}$ .

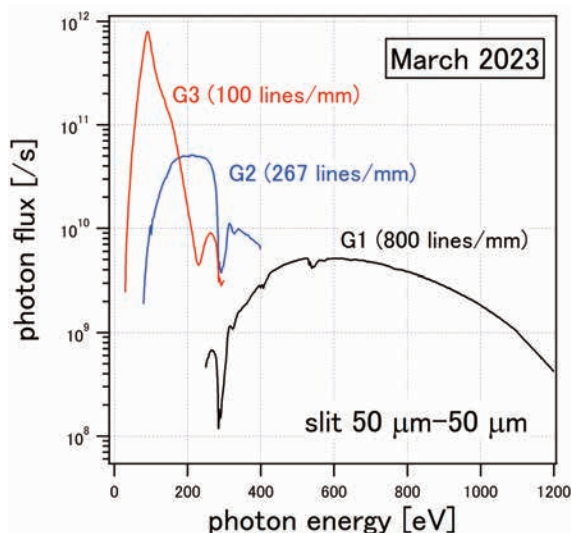


Fig. 1. Photon flux curves for G1, G2 and G3. Entrance and exit slits are set to 50  $\mu\text{m}$ .

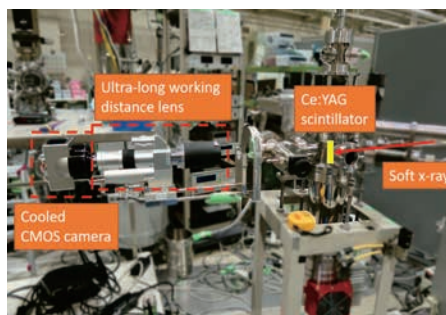


Fig. 2. Photo of focus image measurement equipment at an endstation of BL4B.

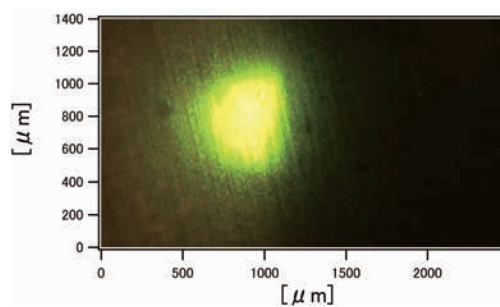


Fig. 3. Focus image at the Ce:YAG scintillator. The photon energy is 400 eV.

BL4B

## Low Radiation Damage XAFS Measurements at BL4B

H. Iwayama<sup>1,2</sup>

<sup>1</sup>UVSOR Synchrotron Facility, Institute for Molecular Science, Okazaki 444-8585, Japan  
<sup>2</sup>School of Physical Sciences, The Graduate University for Advanced Studies (SOKENDAI),  
 Okazaki 444-8585, Japan

Recent developments in synchrotron radiation and focusing optics technologies yield highly brilliant light sources. This high bright synchrotron radiation enables us to measure tiny samples and perform nano-structure analysis such as scanning transmission x-ray microscope (STXM) and photoemission electron microscope (PEEM). In addition, photon-hungry experiments such as resonant inelastic x-ray scattering benefit from the recent higher brightness of synchrotron radiations.

However, the higher brightness causes severe problems of radiation damage to the samples. In particular, soft X-rays has weak penetration power, and only a several-100 nm thickness of the sample almost absorbs them. Thus radiation damage problem for soft X-ray regions is much more severe than that for hard X-ray regions. If a photon flux, focus size, and photon energy are  $10^{13}$  photons/s,  $10\ \mu\text{m}$ , and  $300\ \text{eV}$ , the corresponding dose is estimated to be at  $10\ \text{GGy/s}$  for samples mainly composed of carbon. Critical dose for chemical change are 80, 280, and  $1230\ \text{MGy}$  for polymethyl methacrylate, fibrinogen, and polystyrene, respectively [1]. It means that irradiation of such brilliant synchrotron radiation destroys soft matter samples in a moment.

Low photon flux measurements are also important to avoid radiation damage on fragile samples such as soft matter. In this case, signals of XAFS measurements are weak in proportion to the photon flux. For good SN ratio data, noise levels should be pretty small. A total electron yield (TEY) measurement is one of the most popular X-ray absorption fine structure analysis methods. In the TEY measurements, we measure currents in the sample irradiated by soft X-rays. The current means the total electrons ejected from the sample, corresponding to absorption cross sections. Thus we measure the sample current for each photon energy by using a pico-amperemeter. In this case, the noise of signals mainly comes from electric noise. In particular, noise from the ground level of the experimental hall is critical.

In this work, we estimate radiation damages for XAFS measurements and verify the lower limit of photon flux, which is enough to obtain XAFS spectra with good SN ratios. Our TEY equipment at BL4B is simple. A sample is fixed on a sample holder of an aluminum board in a vacuum chamber using carbon tape. We connect a current output terminal of the vacuum chamber to a pico-amperemeter (Keythley electrometer 617) with a low-noise BNC cable. The sample is  $\text{FePO}_4$  powders.

Figure 1 shows (a) sample currents and (b) the histogram of our TEY equipment when no soft X-ray irradiates the sample. The Full-width half maximum (FWHM) is  $2\ \text{fA}$ . In this measurement, we observe an offset of  $6\ \text{fA}$ . It may be because the ground voltages of the pico-amperemeter and sample holder are slightly different. When we use a standard BNC cable instead of the low-noise cable, the FWHM of noise levels becomes  $2\ \text{fA}$ .

Figure 2 shows TEY spectra of  $\text{FePO}_4$  powders at different photon fluxes. The resolution of photon energies is set to  $E/\Delta E$  of 2000, and it takes 8 minutes to obtain one spectrum. When photon flux is more than  $4 \times 10^7$  photons/sec, SN ratios are enough to find fine structure of XAFS spectra. However, at the photon flux of  $8 \times 10^6$  photons/sec, while we observe the prominent peak at the photon energy of  $710\ \text{eV}$ , sample current intensities are about  $10\ \text{fA}$ , and their fine structures around  $723\ \text{eV}$  are drowned in noise. From this, a lower limit of photon flux is around  $4 \times 10^7$  photons/sec at the Fe L edge, and the corresponding dose is only  $20\ \text{kGy}$ . This work demonstrates that our TEY system enables us to perform low radiation damage XAFS measurements.

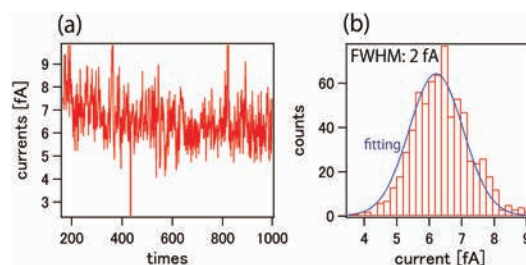


Fig. 1. Noise levels of our TEY equipment at BL4B.

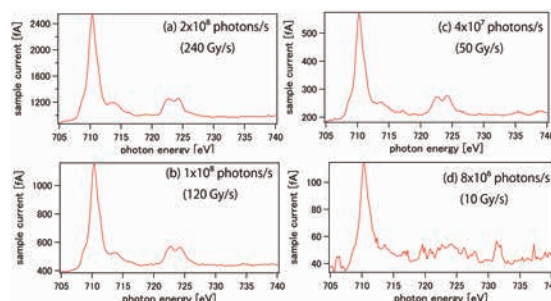


Fig. 2. TEY spectra of  $\text{FePO}_4$  powders for various photon fluxes.

[1] J. Wang *et al.*, J. Electron Spectrosc. Relat. Phenom. **170** (2009) 25.

## Transmission Characteristics of an Optical Filter for UV Observations

A. Yamazaki<sup>1</sup>, K. Goda<sup>1</sup>, T. Matsumoto<sup>2</sup>, S. Teramoto<sup>2</sup> and K. Yoshioka<sup>2</sup>

<sup>1</sup>*Department of Earth and Planetary Science, Graduate School of Science,  
The University of Tokyo, Tokyo 113-0033, Japan*

<sup>2</sup>*Department of Complexity Science and Engineering, Graduate School of Frontier Sciences,  
The University of Tokyo, Chiba 277-8561, Japan*

The hydrogen absorption cell is a unique type of filter that functions as an optical band-stop filter for hydrogen Lyman- $\alpha$ . The Lyman- $\alpha$  is absorbed by hydrogen contained in the cell when thermally dissociated into the atomic state. The shape of this cell is cylindrical ( $\phi 35$  mm, L40 mm), and the windows on each side are made of magnesium fluoride (MgF2) for UV light transmission. Therefore, the cell simply acts as an MgF2 filter without hydrogen gas. Overall, the cell is known for its narrow bandwidth, lightweight, small size, and thus suited to mount on a small spacecraft. We plan to use this filter in the ongoing Comet Interceptor Mission, in which the filter is used to observe the atomic hydrogen coma of the target comet remotely.

However, there is a difficulty regarding this filter: the degradation of MgF2 transmittance. The transmittance of MgF2 drops over time as it alters by UV light irradiation, and this filter is no exception. Since we have been using this filter in past experiments, the center of the MgF2 window is more altered compared to the edges. To better understand the characteristic, in this experiment, we mainly focused on evaluating the position dependence of the MgF2 transmittance and the change in the transmittance after polishing the surface with ethanol. The latter aims to retrieve the transmittance lost due to alteration. Since the experiments aim to understand the characteristics of the filter window, we did not fill hydrogen gas in the cell and thus was not functioning as a band-stop filter.

In the experiment, we measured the position dependence of the filter transmittance. The cell was set on a motorized stage, and the transmittance was measured at multiple incident positions by moving it vertically against the beam. Microchannel plates and a resistive anode encoder were used for the detector. For each measurement, a wavelength scan was performed using the G3M5 grating system with the range of 110-135 nm at an interval of 1 nm. Later, the same measurement was done after polishing the MgF2 surface with ethanol.

Figure 1 shows the transmittance of the cell filter.

The solid and dashed lines show the result before and after polishing the surface with ethanol. The plots' colors describe the different incident positions as shown in the upper right illustration. The area below 116 nm is shaded since the data in this range has a low S/N ratio due to the MgF2 cutoff wavelength at 115 nm.

The result implies that the transmittance increases from the center towards the edge, and also increases by polishing the MgF2 surface with ethanol. However, the increase in transmittance varies significantly among the incident positions. At the center of the cell, the transmittance increases no more than a few percent, but around the edges, it increases by  $\sim 20\%$ . One possible explanation is that polishing the surface is effective for surface dust and smears, but not for degradation caused by intensive UV light irradiation. Since the center of the cell has suffered irradiation throughout the past experiments, the alteration is discernible. Polishing the cell surface proved effective in increasing the transmissions, but we could not fully retrieve those lost due to UV-induced alteration.

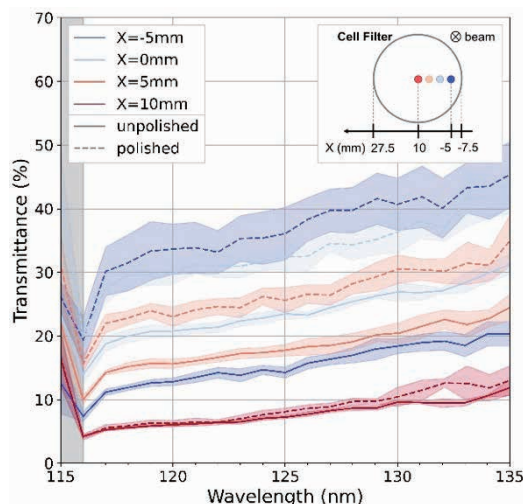


Fig. 1. Transmission spectra of MgF2 windows on a hydrogen absorption cell.

BL5B

## Evaluation of the Pressure Dependence of the Krypton Absorption Cell

M. Kuwabara<sup>1</sup>, K. Kato<sup>1</sup>, K. Arakawa<sup>1</sup> and M. Taguchi<sup>1</sup>

<sup>1</sup>*Department of Physics, College of Science, Rikkyo University, Tokyo 171-8501, Japan*

In planetary upper atmospheres, hydrogen atoms originating from hydrogen molecules in lower atmospheres expand to an altitude equivalent to several planetary radii. These hydrogen atoms resonantly scatter the solar Lyman-alpha radiation (121.567 nm), forming planetary hydrogen coronae. Since the brightness of the hydrogen coronae depends on the number density of hydrogen atoms, the spatial structures can be obtained by imaging the coronae.

A hydrogen absorption cell is efficient tool for remote sensing of the density and temperature distribution of the exospheric hydrogen atoms. Additionally, this technique has advantages over other techniques in terms of geometrical size, weight, and simplicity. Therefore, this technique is expected to be effectively used for exploration using ultra-small spacecraft and other applications [1].

One of the drawbacks of the absorption cell technique is the difficulty of calibration. Since the absorption linewidth of the hydrogen absorption cell is a few pm at most, the calibration system must have high wavelength stability. However, it is revealed that the measurement wavelength of BL5B beam line drifts as the temperature of the mirror changes, so it is necessary to know the correct wavelength for each measurement. This

problem can be overcome by placing a krypton absorption cell in front of the hydrogen absorption cell. This is because krypton has a strong absorption line at 123.584 nm, which is close to the Lyman-alpha line of the hydrogen atom. By measuring the light transmitted through both cells, the peak of the absorption of the hydrogen Lyman-alpha line can be determined.

In this experiment, we evaluate the pressure dependence of the absorption line profile of the krypton cell to establish a calibration method for the hydrogen absorption cell. Figure 1 shows the result of the experiment. The absorption line of krypton is 123.584 nm, but the measurement wavelengths of the calibration system are off, and the peaks are seen a little beyond 124 nm. In addition, the positions of the peak vary in each measurement. Regarding the pressure dependence, as the pressure of krypton gas increases, both the depth and the width of absorption also increase. The result will be used to determine the optimum pressure for the krypton absorption cell needed for the BL5B calibration system in the future.

[1] M. Kuwabara *et al.*, *Rev. Sci. Instrum.* **89** (2018) 023111.

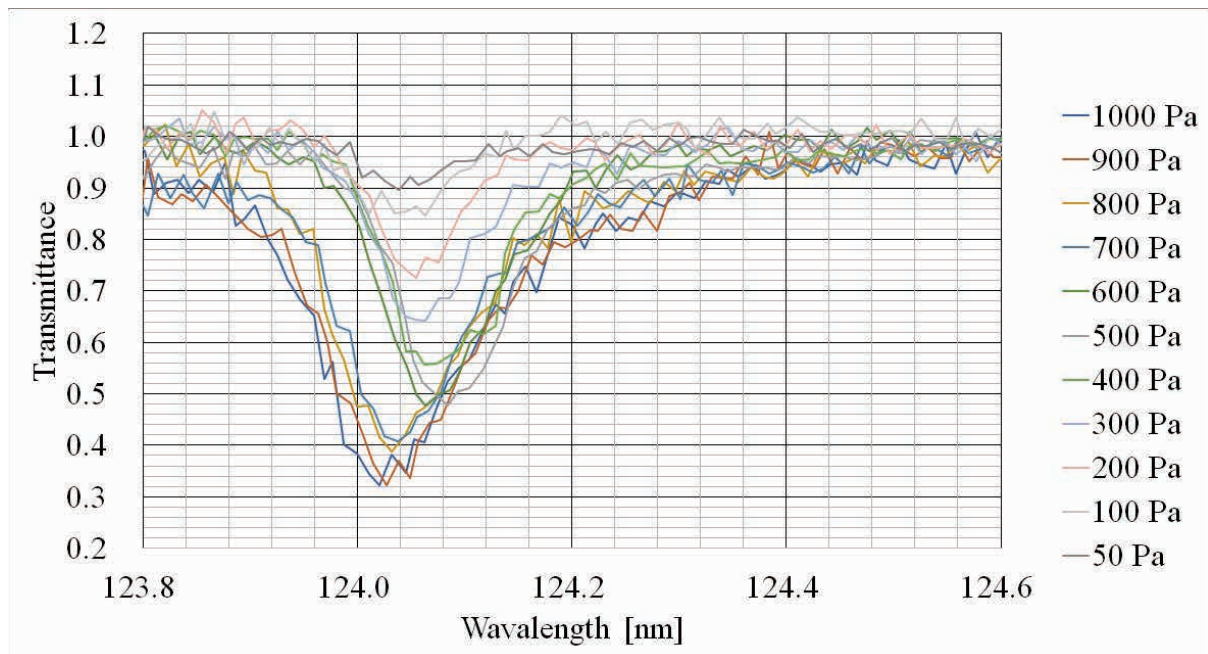


Fig. 1. Pressure dependence of the krypton cell absorption.

## XUV Polarization Measurement using Visible Fluorescence from Neon Atoms

T. Kaneyasu<sup>1,2</sup>, K. Hosaka<sup>3</sup> and J. Adachi<sup>4,5</sup>

<sup>1</sup>SAGA Light Source, Tosu 841-0005, Japan

<sup>2</sup>Institute for Molecular Science, Okazaki 444-8585, Japan

<sup>3</sup>National Institutes for Quantum Science and Technology, Takasaki 370-1292, Japan

<sup>4</sup>Institute of Materials Structure Science, KEK, Tsukuba 305-0801, Japan

<sup>5</sup>The Graduate University for Advanced Studies (SOKENDAI), Tsukuba 305-0801, Japan

Polarization is one of the most important characteristics of synchrotron radiation. For accurate measurements using the polarization properties of synchrotron radiation, it is essential to evaluate the polarization state of light at a sample point. Fluorescence polarimetry is a useful technique to determine the polarization state of the extreme ultraviolet (XUV) radiation. This method is based on the conversion of XUV radiation to visible light on the atomic resonance [1,2]. The fluorescence preserves the polarization state of the excitation light when it is observed along the light propagation axis. Comparing with the optical polarimeters [3,4], this method has advantages in its simple apparatus and easy operation. Up to the present, however, this method has been only applied to helium atoms [2,4,5], and the wavelength range is restricted to around 50 nm. In this study, we show that neon atoms can be used to measure the polarization state of XUV radiation at 60 nm wavelength.

The experiment was performed at the bending magnet beamline BL5B. Figure 1 shows the experimental layout of the present study. The wavelength of monochromatized synchrotron radiation was set to 59.6 nm. Neon atoms were provided by an effusive beam. The XUV radiation resonantly excites the neon atom to the  $4d^1[3/2]_1$  state. This state decays to the  $3p[1/2]_1$  state with the emission of 511.4 nm fluorescence photon. The fluorescence photons emitted parallel to the light propagation axis ( $z$ -axis) were detected by a photomultiplier tube equipped with a polarizer and a bandpass filter. The fluorescence photon basically preserves the polarization state of the XUV radiation. The only difference between them is that the polarization angle of the fluorescence photon is expected to rotate by 90 degrees with respect to the polarization angle of the incident XUV radiation.

Figure 2 shows the fluorescence intensity measured as a function of the polarizer angle which is defined by the angle of the polarization axis with respect to the horizontal axis ( $x$ -axis). In accordance with the expectation, the fluorescence intensity shows a sinusoidal modulation reflecting the vertically linear polarization of the fluorescence photon. Assuming an elliptical polarization, the experimental data points are

fitted by a theoretical curve. The linear polarization degree and polarization angle of XUV radiation are evaluated to be  $0.67 \pm 0.02$  and  $10 \pm 2$  degrees, respectively. This is roughly in agreement with the results obtained by helium atoms [5, 6], suggesting the capability of fluorescence polarimeter using neon atoms.

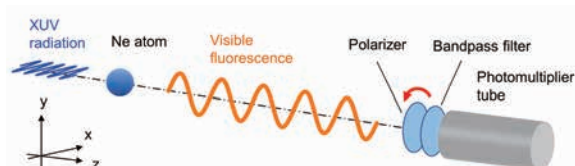


Fig. 1. Experimental setup. The visible fluorescence photon emitted along the light propagation axis was detected.

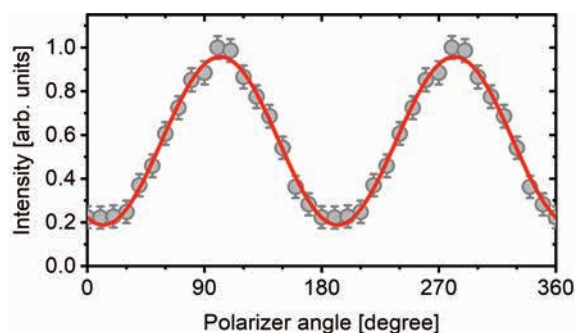


Fig. 2. Fluorescence intensity measured as a function of the polarizer angle. The experimental data points are fitted by a theoretical curve.

[1] V. Bobahev and O. S. Vasyutinskii, *Rev. Sci. Instrum.* **63** (1992) 1509.

[2] C. J. Latimer *et al.*, *J. Electron Spectroscopy Relat. Phenom.* **101-103** (1999) 875.

[3] D. Cubric *et al.*, *Meas. Sci. Technol.* **10** (1999) 554.

[4] E. Allaria *et al.*, *Phys. Rev. X* **4** (2014) 041040.

[5] T. Kaneyasu, K. Hosaka and J. Adachi, *UVSOR Activity Report 2020* **49** (2021) 46.

[6] Y. Hosaka, H. Iwayama and T. Kaneyasu, *J. Synchrotron Rad.* **27** (2020) 675.

BL5B

## A Position-sensitive Microchannel Plate Detector with Resistive Anode

S. Matoba<sup>1</sup>, S. Kanda<sup>1</sup>, H. Ohshita<sup>1</sup>, K. Hirata<sup>2</sup>, H. Iwayama<sup>3,4</sup> and T. Kaneyasu<sup>5</sup>

<sup>1</sup>*Institute of Materials Structure Science, KEK, Tsukuba 305-0801, Japan*

<sup>2</sup>*National Metrology Institute of Japan, National Institute of Advanced Industrial Science and Technology, 1-1-1 Higashi, Tsukuba, Ibaraki 305-8565, Japan*

<sup>3</sup>*Editorial Board, UVSOR Synchrotron Facility, Institute for Molecular Science, Okazaki 444-8585, Japan*

<sup>4</sup>*School of Physical Sciences, The Graduate University for Advanced Studies (SOKENDAI), Okazaki 444-8585, Japan*

<sup>5</sup>*SAGA Light Source, Tosu 841-0005, Japan*

A microchannel plate (MCP) is a lead glass detector with a two-dimensional array of electron-multiplying pores of about 10  $\mu\text{m}$  in diameter. When charged particles or short-wavelength photons collide with the inner wall of the pore, secondary electrons are generated and amplified in the pore to be detected as electron pulses. MCPs are used in a very wide range of fields from basic research to industry because of their large area, high spatial resolution, and high-speed detection capability.

We are developing a system that enables easy measurement of imaging techniques using quantum beams regardless of the beam type and location, which can be used for trial experiments prior to the use of advanced devices. The most common method of two-dimensional detectors for MCP anodes is optical detection of emission from fluorescent anodes using a CCD camera or the like. However, the difficulty of inserting a detector in the middle of the beamline and the upper limit of the frame rate of the camera limit the use of this method for accelerator beamlines. Another major method, the delay-line anode[1], requires a high-speed circuit that can detect time differences between wires, making it expensive and difficult to implement in small-scale experiments.

We are developing a position-sensitive detector using resistive anodes as a two-dimensional detector for various particles such as neutrons, ultraviolet light, muons, and ions. The advantages of this system are that position detection can be easily performed by using a 4-channel waveform analyzer and that the resistive anodes are only about 2 mm thick, so they can be assembled into a compact assembly. Resistive anodes as two-dimensional detector elements have been developed for a long time[2], but there is no simple system that can be used by researchers who are not detector experts, and we are developing one.

In this experiment, the “solid chamber” of BL5B was removed and a pinhole, a four-quadrant slit, and a light-reducing filter made of aluminum foil and tungsten mesh were installed to detect the incident position of

the MCP with a wavelength of 130 nm UV light of approximately 1 mm in diameter. The charge of the electron pulses generated by the MCP, which has an effective diameter of 40 mm and consists of two stages, is dispersed and transferred to the electrodes at the four corners of the resistive anode. The two-dimensional position information is calculated from the current flowing to each electrode as  $x/d = (I_1 + I_4) / I$ ,  $y/d = (I_1 + I_2) / I$  (where  $d$  is the full width or height of one side of the resistive anode and  $I = I_1 + I_2 + I_3 + I_4$ ). The current flowing to each electrode was measured with a 4-channel amplifier, shaper and waveform analyzer.

Figure 1 shows an example of the measured light positions. In this experiment, the measurement system was verified and confirmed to be capable of sound position detection. In the future, the position resolution and detection efficiency distribution will be investigated using patterns, etc.

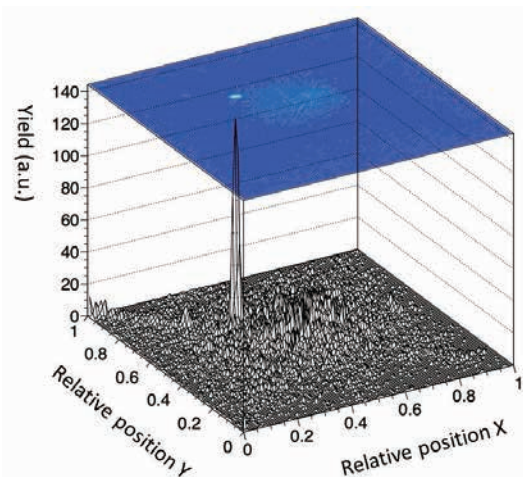


Fig. 1. Position reconstruction on the resistive anode.

[1] S. E. Sobottka and M. B. Williams, *IEEE Trans. Nucl. Sci.*, **35** (1988) 348.

[2] M. Lampton and R. F. Malina, *Rev. Sci. Instrum.*, **47** (1976) 1360.

## Progress of Photoelectron Momentum Microscopy for Revealing Complex and Detailed Electronic Structures of Materials

S. Suga<sup>1,2</sup> and F. Matsui<sup>3,4</sup>

<sup>1</sup>SANKEN, Osaka University, Osaka, 567-0047, Japan

<sup>2</sup>PGI-6, Jülich Research Center, Germany

<sup>3</sup>UVSOR Synchrotron Facility, Institute for Molecular Science, Okazaki 444-8585, Japan

<sup>4</sup>The Graduate University for Advanced Studies (SOKENDAI), Okazaki 444-8585, Japan

The photoelectron momentum microscope (often abbreviated as 2D-PMM) is installed already in 2020 at BL6U of UVSOR in the form of single hemispherical deflection electron energy analyzer (HDA) behind the PEEM type objective lens, which can easily be switched between the real space to the momentum space detection mode.  $E_B(x,y)$  or  $E_B(kx,ky)$  constant energy contour (CEC) can be simultaneously detected by a 2D detector behind the focusing lens optics installed after the exit of the HDA[1]. The detection efficiency of the  $E_B(kx,ky)$  is very high in comparison with the conventional HDA detection due to the simultaneously covered wide acceptance angle owing to the use of PEEM, where the sample rotation is not necessary for  $E_B(kx,ky)$  detection and excitation light focusing is not necessary to probe micro-nano regions. Then very reliable gigantic data set is obtained by this instrument in rather short measuring time [2–4]. Temperature down to 10 K can be measured.

Since the best quality sample surface region down to  $\sim 10 \mu\text{m}$  can be selected by the proper sized field aperture in the objective lens, high quality and reproducible data can be obtained by this instrument. The beam focusing is not necessary in this system by using the PEEM and several tens of nm resolution can be realized without noticeable radiation damage.

Detailed behaviors of CECs of graphite are shown in Fig.1 [3]. Resolutions are  $\Delta E \sim 40 \text{ meV}$  and  $\Delta k \sim 0.01 \text{ \AA}^{-1}$ . Band dispersions along any  $kx$ - $ky$  direction can be immediately derived from the big data.

Since 2022 upgrading is progressing. In addition to  $68^\circ$  incidence of light from the surface normal direction,  $0^\circ$  incidence is soon available. HDA is upgraded to 2 HDAs to realize this configuration. 2D spin filter will be installed within a few months to realize the multichannel figure of merit  $\text{FoM} \sim 10^2$ . Then the spin detection efficiency becomes  $10^4$  times higher than the single channel spin detection and  $10^2$  times higher than using the W (tungsten) 2D spin filter.

Various additional upgrading of the SP-2D-PMM system in UVSOR will be made in the next few years, producing the world best heavy data on micro-nano regions of exotic and/or functional materials supporting the new device development.

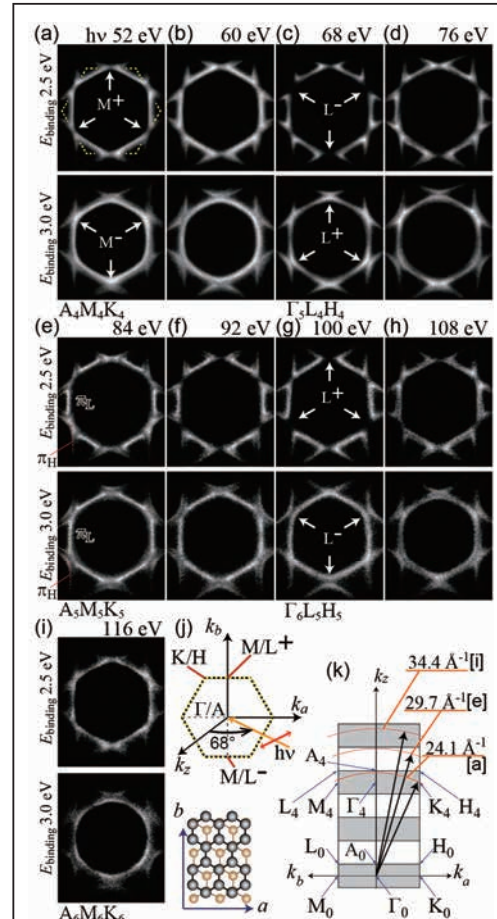


Fig.1. CECs of graphite (0001) at various  $h\nu$  reproduced from Ref.[3]. Thus  $E_B(kx,ky,kz)$  as well as band dispersions along any  $kx$ - $ky$  directions can be easily derived from gigantic data.

[1] S. Suga, A. Sekiyama, C. Tusche, Photoelectron Spectroscopy, Springer, Springer Series of Surface Science **72** (2021) 1–503.

[2] F. Matsui, S. Makita, H. Matsuda, T. Yano, E. Nakamura, K. Tanaka, S. Suga, and S. Kera, Jpn. J. Appl. Phys. **59** (2020) 067001.

[3] F. Matsui and S. Suga, Phys. Rev. B **105** (2022) 235126.

[4] F. Matsui, Y. Okano, H. Matsuda, T. Yano, E. Nakamura, S. Kera and S. Suga, J. Phys. Soc. Jpn. **91** (2022) 094703.

BL6B

## Low-frequency Photocurrent Response in Semiconductors Based on ns-visible-pump broadband-infrared-probe Spectroscopy

J. Nishida<sup>1\*</sup> and T. Kumagai<sup>1</sup><sup>1</sup>Institute for Molecular Science, National Institutes of Natural Sciences, Okazaki 444-8585, Japan

Optical responses of photoinduced carriers in mid- to far-infrared encode their scattering times as well as trap and polaronic states, which are all directly relevant to the mobility of the carriers. Yet, due to the spectrally broad nature of such responses, the time-resolved study of such photoinduced carriers is often difficult and requires advanced laser sources for ultrafast experiments [1]. While mid-infrared thermal light source with fast electronics covers important subsets of the spectral range and time resolution [2], the full characterization of the low-frequency carrier response has remained elusive.

An extremely broadband output of a synchrotron provide unique opportunities to tackle such problems. With the combination of broad spectrum extending from mid- ( $\sim 100$  meV) to far-infrared ( $\sim$  meV), as well as a reasonable pulse duration of  $< 1$  ns, it may be possible to address the scattering and polaronic stabilization of photoinduced carriers on the nanosecond time scale. Such an information is particularly relevant to address the photoinduced carrier responses in lead halide perovskites, where the interaction of carriers with surrounding lattice has been intensely debated [3].

We thus attempted to combine the mid-infrared synchrotron output at BL6B beam line as a probe pulse with a 10s-ns visible laser as a pump pulse (Fig. 1a). We mainly focused on the application in the single-bunch operation ( $\sim 5$  MHz) to enforce the relaxation of photoinduced carriers as much as possible. The TTL output synchronized with the synchrotron laser is used to trigger our commercial and duration-tunable (6 – 40 ns) pulsed nanosecond laser. In collaboration with Equipment Development Center, we developed time-delay generator and modulator to control the timing between the visible and broadband mid-infrared pulse, as well as to modulate the visible pump pulse intensity. The modulation frequency is used for the lock-in detection of the photoinduced change in the intensity that transmits a sample. We implemented a Michelson interferometer for spectral measurements.

We first demonstrated the photo-modulation absorption spectroscopy on the low-frequency response of silicon. In Fig. 1b, we show an acquired interferogram in the ground-state ( $I$ ), and its photoinduced change ( $\Delta I$ ). With the average time of  $\sim 30$  min, we demonstrated the sensitivity of  $\Delta I/I \sim 10^{-3}$ . The Fourier transform (Fig. 1c) shows the divergent response toward the low-frequency side, consistent with the Drude-like behavior

expected for the photo-carriers in silicon.

We then attempted to extend the approach to perovskite quantum dots dispersed in solution. While we observed a photoinduced change in the transmitted intensity, the response was strongly dependent on the modulation frequency (Fig. 1d), likely pointing to a thermal effect. Such a thermal contribution can be alleviated by modulating the pump pulse rapidly at 100 kHz. We scanned the pump-probe delay to identify any relaxation processes related to the photoinduced carriers, but so far could not identify any such responses (Fig. 1d, inset; 5 min average each point).

To observe photoinduced carriers in a broad range of semiconductor materials, we estimate another order of magnitude improvement is necessary for the signal-to-noise ratio. We confirmed that the current signal-to-noise level is limited by the HgCdTe detector, potentially due to the large element size. With the optimization of the electronics, we may attain enough sensitivity to be combined with the time resolution and spectral range that we demonstrated.

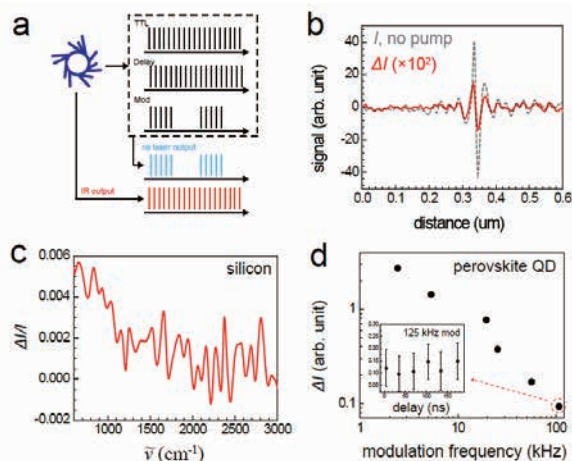


Fig. 1. (a) Timing scheme, (b) photo-modulated interferogram and (c) spectrum on silicon, (d) modulation-frequency dependence of photo-induced modulation.

[1] T. T. Yeh *et al.*, *Sci. Rep.* **7** (2017) 1.

[2] K. Furuhashi *et al.*, *J. Phys. Chem. C* **117** (2013) 19101.

[3] K. Munson T. *et al.*, *Chem*, **4** (2018) 2826.

## Study on the Reflective Properties of Black Coatings Used in UV Observation Equipment.

T. Matsumoto<sup>2</sup>, K. Goda<sup>1</sup>, A. Yamazaki<sup>1</sup>, K. Inoue<sup>1</sup>, S. Liu<sup>2</sup> and K. Yoshioka<sup>2</sup>

<sup>1</sup>Department of Earth and Planetary Science, Graduate School of Science,

The University of Tokyo, Tokyo 113-0033, Japan

<sup>2</sup>Department of Complexity Science and Engineering, Graduate School of Frontier Sciences,

The University of Tokyo, Chiba 277-8561, Japan

The emission angle dependence of scattered light intensity (Experiment 1) and reflectance (Experiment 2) were measured for three different, black-coated aluminum plates (Samples A, B, and C) and a mirror. The reflectance of the samples was determined based on their relative reflectance to the mirror. This experiment aimed to optimize the black coating to be applied to the optics of the hydrogen imager (HI) on board the Comet Interceptor (CI) mission to be launched in 2029. To do this, we quantitatively determine the black coating that minimizes stray light caused by reflections inside the equipment. These measurements are also crucial for the quantitative estimation of the expected performance of CI/HI.

The setup for both Experiment 1 and Experiment 2 was the same. Samples A, B, and C and a mirror were mounted on the inner rotating stage, while the detector was mounted on the outer rotating stage (Fig. 1). The detector used was a photodiode with an effective area of 10 mm × 10 mm. The slit width was adjusted to prevent saturation of the measured values at each incident angle. A G3 diffraction grating was used.

The following 12 measurements were performed.

$$\begin{array}{|c|} \hline 4 \text{ targets} \\ \hline (A, B, C, \text{Mirror}) \\ \hline \end{array} \times \begin{array}{|c|} \hline 3 \text{ incident angles} \\ \hline (30^\circ, 45^\circ, 60^\circ) \\ \hline \end{array}$$

In Experiment 1, the wavelength was set to 121.4 nm. The detector was positioned with the direction of the incoming beam as 0° and rightward as positive. Angle scans were performed from 45° to 180° with an interval of about 13.5°, followed by angle scans near the peak with an interval of about 2°. In Experiment 2, the detector was fixed, and wavelength scans were performed from 112 nm to 133 nm with an interval of 1 nm without summing.

Experiments 1 and 2 are summarized below with their results (Fig. 2 and Fig. 3).

The results found that, at any incident angle, the reflectance was A, B, and C from the lowest to the highest, with Sample A being the most optimal. However, the reflectance of Samples A and B was negative only at 45° incident angle, which might have been due to the dark noise and the positional accuracy of the detector. Further experiments are needed to confirm reproducibility and evaluate the consistency of the incident angle dependence of reflectance with theoretical values.

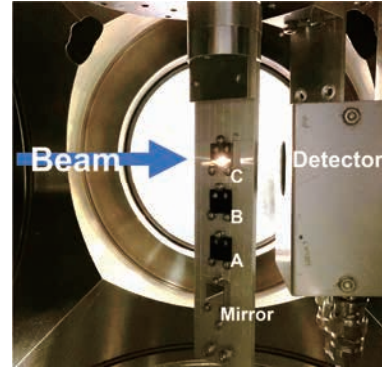


Fig. 1. The setup of the measurements.

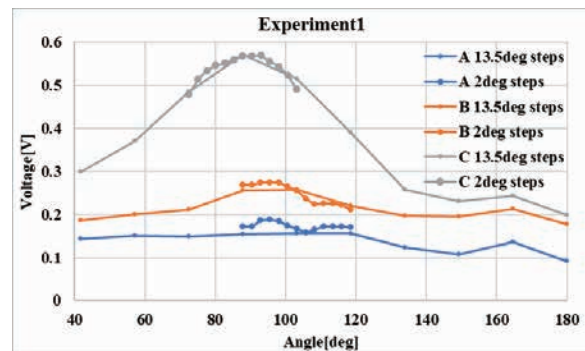


Fig. 2. Experiment 1: The emission angle dependence of the scattered light intensity

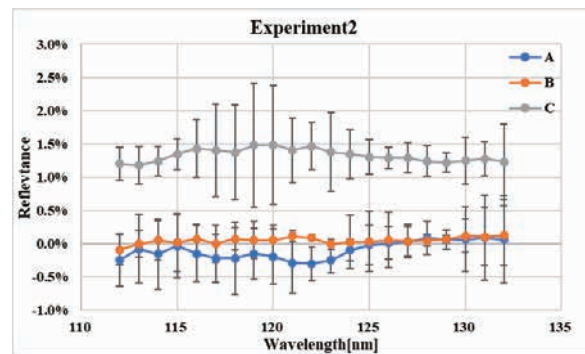


Fig. 3. Experiment 2: Reflectance

BL7B

## Complex Refractive Index Measurement by Reflectance Spectra in Different Polarization Configurations (II)

K. Shinkai<sup>1</sup>, K. Fukui<sup>1</sup>, K. Yamamoto<sup>1</sup> and T. Saito<sup>2</sup>

<sup>1</sup>Department of Electrical and Electronics Engineering, University of Fukui, Fukui 910-8507, Japan

<sup>2</sup>Department of Electrical and Electronic Engineering, Tohoku Institute of Technology, Sendai 982-8577, Japan

Based on the basic design of the instrument by a group at AIST [1], a combined refractive index spectrum measurement system (CRIMS-VUV) [2] has been developed specifically for BL7B, which can continuously measure from the visible region (VIS) at 2 eV to the vacuum ultraviolet (VUV) region at 20 eV. CRIMS-VUV is composed of two measurement modes (spectroscopic ellipsometry measurement (SE) mode and reflection spectrum measurement (OR) mode), both of which can be performed in the same environment.

SE mode has the advantage of measuring the complex refractive index with high accuracy. However, this mode has the disadvantage that, due to its measurement principle, it takes time to measure at each measurement point (photon energy), making it difficult to measure a continuous spectrum. In this respect, OR mode is suitable for measuring continuous spectrum. The well-known Kramers - Kronig analysis (KKA) method is used to determine the complex refractive index spectrum from the reflectance spectrum. However, as mentioned our previous work [2], KKA method is useful, for example, for obtaining qualitative complex refractive index spectrum for limited photon energy region around the absorption edge, but is not well suited for obtaining quantitative complex refractive index spectrum over a wide photon energy region. Therefore, we decided to use the method for determining the complex refractive index from the reflectance in *p*- and *s*-polarization configurations (PS method) as a method for determining the complex refractive index from the reflectance for each photon energy. This method requires the linear polarization of the incident light (Stokes parameter  $S_1$ ), which can be measured from the SE mode of the system. The  $S_1$  can be measured from the SE mode of the system, and the polarization

configuration can be easily changed with the system. These features make the PS method suitable for this system. The following are the intermediate results of complex refractive index measurements of fused silica glass substrate using this PS method.

Figure 1 shows reflectance spectra both in *p*- and *s*-polarization configurations. The dots are reference points which represent the reflectance calculated from the complex refractive index obtained from the ES mode, and the lines are reflection spectra of the OR mode in *p*- and *s*- polarization configurations corrected for the reference points. Note that the effect of surface roughness is taken into account in the optical model of the ES mode and reflectance calculations. The dispersion after the band edge is well shown by the continuous spectrum.

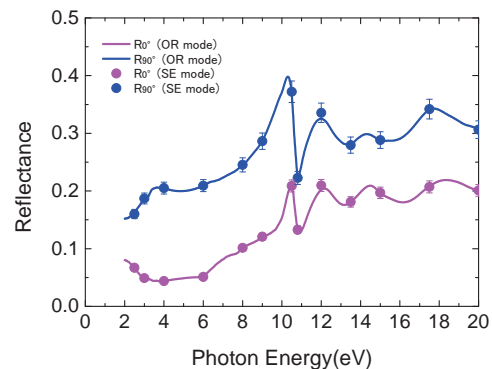


Fig. 1. Reflectance spectra in *p*- and *s*-polarization configurations of fused quartz glass

[1] T. Saito, M. Yuri and H. Onuki, Rev. Sci. Instrum. **66** (1995) 1570.

[2] M. Horiba *et al.*, UVSOR Activity Report 2021 **49** (2022) 49.

## Performance of the Refreshable Large Crystal Nuclear Emulsion for the NINJA Experiment

T. Fukuda<sup>1,2</sup>, H. Kobayashi<sup>2</sup>, Y. Hirobe<sup>2</sup>, Y. Morimoto<sup>2</sup> and M. Nakamura<sup>1,3</sup>

<sup>1</sup>*F-lab., Graduate School of Science, Nagoya University, Nagoya 464-8602, Japan*

<sup>2</sup>*Institute for Advanced Research, Nagoya University, Nagoya 464-8601, Japan*

<sup>3</sup>*Institute of Materials and Systems for Sustainability, Nagoya University, Nagoya 464-8601, Japan*

In neutrino oscillation studies, it is important to detect short-range hadrons in the energy range of about 1 GeV in order to understand neutrino-nucleus interactions. The Emulsion Cloud Chamber (ECC) is a sandwich structure consisting of a special photographic film nuclear emulsion film with sensitivity to minimum ionizing particles, with a thickness of several hundred microns (composed of two sensitive emulsion gel layers each tens of microns thick and plastic base layer), and a thin target material with a thickness of several hundred microns to several millimeters, stacked alternately. The NINJA experiment, which uses ECC as the main detector, has been publishing measurement data on low-energy hadrons for neutrino-iron and neutrino-water interactions since 2014, while expanding the scale of the experiment.

This autumn to winter, we plan to conduct a large-scale statistical experiment on neutrino-H, O, C, and Fe nuclear interactions using about 250 square meters of nuclear emulsion films. The tracks on the nuclear emulsion films are automatically scanned by the track selecting device HTS, but 250 square meters is twice the amount of the previous experimental run that took approximately 20 months for track scanning, and we are developing the track selecting device HTS2, which has five times the scanning speed of HTS. With the expansion of the field of view, the pixel size of HTS2 has been increased, and it is necessary to increase the size of the developed silver grains compared to the conventional nuclear emulsion.

We have created a nuclear emulsion with AgBrI crystal size of 320 nm, which is larger than the conventional 240 nm, and added a group of chemicals that have a proven effect in suppressing latent image fading and fogging. After irradiating the emulsion films with electron beams using UVSOR, we performed a refresh process to eliminate unwanted tracks by exposing it to high temperature and humidity conditions (30°C, 95%RH). We have newly discovered that the refresh which removes unwanted tracks is insufficient (Fig. 1.). The left image of Fig. 1. has a grain density of  $53.5 \pm 1.5$  grains/100  $\mu\text{m}$  and has not undergone a refresh process. The image on the right of Fig. 1. has undergone a refresh process with a grain density of  $29.8 \pm 1.7$ , but the disappearance of tracks due to the refresh process is insufficient.

Based on our experience in the OPERA experiment, we conducted experiments to determine the appropriate

amount of 5-methylbenzotriazole (5-MBT, Fig. 2.), which promotes refreshment by oxidizing latent image nuclei in high humidity conditions. The results of comparing the GD of emulsion film samples with varying amounts of 5-MBT added, using UVSOR to apply an electron beam and comparing with and without refresh processing, are shown in Fig. 3. The initial sensitivity decreased depending on the amount of 5-MBT added to the emulsion. However, when 5-MBT was added at  $1.0 \times 10^{-3}$  or more moles per mole of silver in the emulsion, the refresh effect was enhanced. A suitable amount of balance between the refresh effect and initial sensitivity was found through this addition.

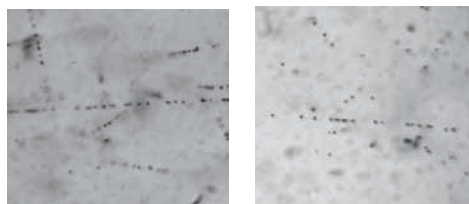


Fig. 1. Microscopic images of large crystal emulsion films. (left) unrefreshed film. (right) refreshed film.

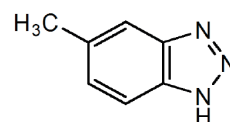


Fig. 2. The chemical formula of 5-MBT.

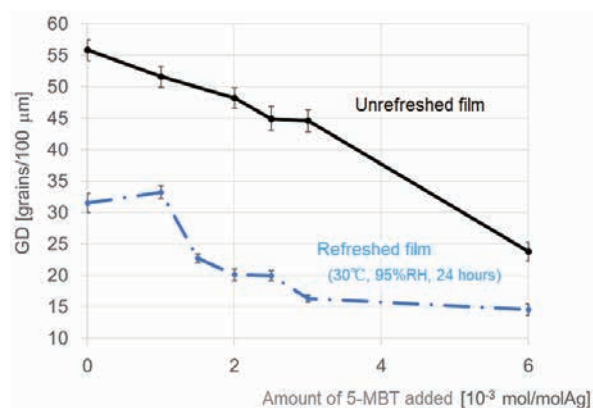


Fig. 3. GD of electron beam tracks. The solid and dashed lines show the data of unrefreshed films and refreshed films, respectively.

## Lattice Design of the UVSOR-IV Storage Ring

E. Salehi<sup>1</sup>, Y. Taira<sup>1</sup>, M. Fujimoto<sup>1,3</sup> and M. Katoh<sup>1,2</sup>

<sup>1</sup>UVSOR Synchrotron Facility, Institute for Molecular Science, Okazaki 444-8585, Japan

<sup>2</sup>Hiroshima Synchrotron Radiation Center, Hiroshima University, Higashi-hiroshima 739-0046, Japan

<sup>3</sup>NUSR, Nagoya University, Nagoya, Japan

In this study, we have designed a new lattice for UVSOR storage ring to provide diffraction-limited light in the vacuum ultraviolet range which requires a small emittance at least a few nm. UVSOR is a low energy synchrotron light source. After some major upgrades [1-4], it is now called UVSOR-III, which has a moderately small emittance of about 17 nm and provide vacuum ultraviolet light of high brightness.

In order to provide diffraction-limited light, at the first step, we have analyzed the present magnetic lattice of UVSOR based on tie diagram to explore the possibility to get a lower emittance with some minor changes in the configuration of magnets. We have found a few optics which has smaller emittance around 10 nm than the present value [5]. To reach the low emittance around a few nm, we have designed a new storage ring of 1 GeV electron energy, which is higher than the present value, 750 MeV. The magnetic lattice is based on a compact double bend achromat cell. This cell consists of two bending magnets and four focusing magnets, all of which are of combined function magnets. In this lattice two sextupole families are located in between two combined dipoles for the chromaticity correction and two harmonic sextupole families are also employed to correct the high order geometric aberrations. The circumference is 82.5 m. This lattice has twelve DBA cells with six long straight sections about 4 m and six short straight sections around 1.5 m long. Among 12 straight sections, two sections will be used for the injection and RF cavity, and ten sections will be used for insertion devices. These lengths are same as those of UVSOR-III. This may enable us to use the undulators at UVSOR\_III in the new ring. The undulators can radiate nearly diffraction-limited light in VUV.

A tune survey was performed to optimize the magnet arrangement and the working point by ELEGANT [6]. We found an optic with a small natural emittance around 4.2 nm in the achromatic condition, which becomes lower in the non-achromatic condition. Occupying three short straight sections with 2T multipole wigglers in symmetry can reduce the emittance to 3.6 nm-rad. Moreover, these wigglers provide intense tender X-rays. Figure 1 shows (left) the lattice functions in the achromatic condition and (right) the dynamic aperture for on- and off energy particles at the straight section after optimizing the strengths of the harmonic sextupoles.

Intra-beam and Touschek scattering which dominate the lifetime in low emittance storage rings, particularly of low energy has been studied. Figure 2 shows that IBS effect increases the Touschek lifetime, while the

emittance is increased. One possible technique to decrease the IBS effect is lengthening the bunches by using harmonic cavity which is routinely used at UVSOR-III. Our simulation shows that the increasing of the bunch length by 80 mm can reduce IBS effect on the emittance to an acceptable level with to  $\epsilon_0 = 4.3 \text{ nm}$  [7].

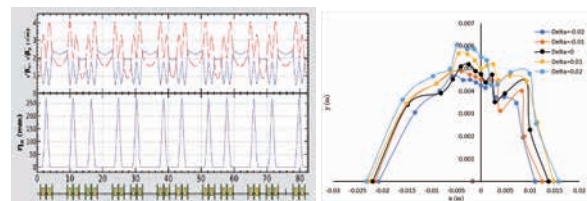


Fig. 1. (Left) Lattice function of 1 GeV storage ring with a small emittance of 4.2 nm for UVSOR-IV, (right) dynamic aperture of optic for different energy deviation.

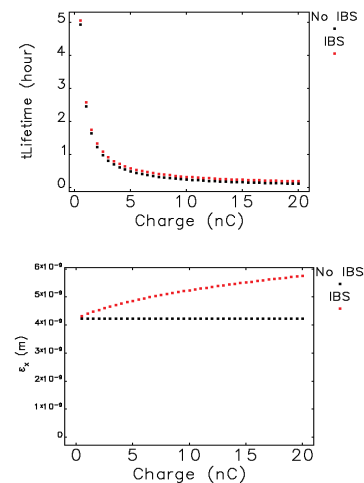


Fig. 2. IBS effect on Touschek lifetime (top) and longitudinal emittance (bottom) versus bunch charge.

- [1] M. Katoh, K. Hayashi, *et al.*, *Nucl. Instr. Meth. A* **467** (2001) 68.
- [2] M. Katoh, M. Hosaka, *et al.*, *AIP Conf. Proc.* **705** (2004) 49
- [3] M. Adachi, H. Zen, *et al.*, *J. Phys. Conf. Ser.* **425** (2013) 042013.
- [4] M. Katoh, M. Adachi, *et al.*, *AIP Conf. Proc.* **1234** (2010) 531.
- [5] E. Salehi and M. Katoh, in *Proc. IPAC'21*, Campinas, Brazil, May 2021, 3970.
- [6] M. Borland, APS LS-287 (2000). <https://www.aps.anl.gov/Accelerator-Operations-Physics/Software>
- [7] E. Salehi, Y. Taira, *et al.*, *J. Phys. Conf. Ser.* **2420** (2023) 012062.

# UVSOR User 3

